HHS Public Access

Author manuscript

*Sci Signal*. Author manuscript; available in PMC 2022 April 19.

Published in final edited form as:

*Sci Signal*. 2021 October 19; 14(705): eabc4764. doi:10.1126/scisignal.abc4764.

# The injury response to DNA damage in live tumor cells promotes anti-tumor immunity

**Ganapathy Sriram**[a,b,c,d,&], **Lauren E. Milling**[a,d,&], **Jung-Kuei Chen**[a,b,c,d], **Yi Wen Kong**[a,b,c,d], **Brian A. Joughin**[a,c,d], **Wuhbet Abraham**[d], **Susanne Swartwout**[a,b,c,d], **Erika D. Handly**[a,c,d], **Darrell J. Irvine**[a,d,f,g,h,*], **Michael B. Yaffe**[a,b,c,d,e,*]

[a]Department of Biological Engineering, Massachusetts Institute of Technology, Cambridge, MA 02142

[b]Department of Biology, Massachusetts Institute of Technology, Cambridge, MA 02142

[c]Center for Precision Cancer Medicine, Massachusetts Institute of Technology, Cambridge, MA 02139

[d]David. H. Koch Institute for Integrative Cancer Research, Massachusetts Institute of Technology, Cambridge, MA 02139

[e]Divisions of Acute Care Surgery, Trauma, and Surgical Critical Care and Surgical Oncology, Department of Surgery, Beth Israel Deaconess Medical Center, Harvard Medical School, Boston, MA 02215

[f]Department of Materials Science and Engineering, Massachusetts Institute of Technology, Cambridge, MA 02139, USA

[g]The Ragon Institute of Massachusetts General Hospital, Massachusetts Institute of Technology and Harvard University, Cambridge, MA 02139, USA

[h]Howard Hughes Medical Institute, Chevy Chase, MD 20815, USA

## Abstract

Although immune checkpoint blockade (ICB) has strong clinical benefit for treating some tumor types, it fails in others, indicating a need for additional modalities to enhance the ICB effect. Here, we identified one such modality by using DNA damage to create a live, injured tumor cell adjuvant. Using an optimized ex vivo co-culture system, we found that treating tumor cells with specific concentrations of etoposide, mitoxantrone, or doxorubicin markedly enhanced

[*]Corresponding authors: djirvine@mit.edu) (D.J.I.) and myaffe@mit.edu (M.B.Y.).

[&]These authors contributed equally to this work

**AUTHOR CONTRIBUTIONS:** GS and MBY conceived the study, designed the experiments, interpreted the results and wrote the manuscript. MBY also obtained funding for the study. DJI interpreted the results, designed experiments and supported the study with funding. GS and LEM designed and performed the experiments, analyzed the data and interpreted the results. LEM also contributed to writing the manuscript. JC generated a stable cell line for the study and prepared figures. YWK and EDH performed specific experiments. YWK also analyzed data and prepared figures. WA helped with animal colony maintenance. SS helped prepare the model figure. BAJ provided critical input on the statistical tests used.

**Competing interests:** G.S., L.E.M., D.J.I., and M.B.Y. are inventors on patent application PCT/US2020/052775 submitted by MIT that covers the use of live chemotherapy-injured cells as an immune adjuvant for immunotherapy of cancer. The other authors declare that they have no competing interests.

**Data and materials availability:** All data needed to interpret the study's findings are present in the main or supplemental files.

dendritic cell–mediated T cell activation. These immune-enhancing effects of DNA damage did not correlate with immunogenic cell death markers or with the extent of apoptosis or necroptosis; instead, these effects were mediated by live injured cells with activation of the DNA-PK, ATR, NF-κB, p38 MAPK, and RIPK1 signaling pathways. In mice, intra-tumoral injection of ex vivo etoposide–treated tumor cells in combination with systemic ICB (by anti-PD1 and anti-CTLA4 antibodies) increased the number of intra-tumoral $CD103^+$ dendritic cells and circulating tumor-antigen–specific $CD8^+$ T cells, decreased tumor growth, and improved survival. These effects were absent in *Batf3*$^{-/-}$ mice and in mice in which the DNA-damaging drug was injected directly into the tumor, due to DNA damage in the immune cells. The combination treatment induced complete tumor regression in a subset of mice that were then able to reject tumor re-challenge, indicating that the injured cell adjuvant treatment induced durable anti-tumor immunological memory. These results provide a strategy for enhancing the efficacy of immune checkpoint inhibition in tumor types that do not respond to this treatment modality by itself.

## INTRODUCTION

Cytotoxic chemotherapy remains a mainstay of cancer treatment. It is estimated that >60% of all cancer patients will receive some type of initial treatment beyond surgery that includes DNA damaging drugs and/or anti-microtubule agents, particularly in patients with more advanced stage disease (1). These conventional chemotherapy treatments result in extended survival and/or cure, depending on the specific tumor type; however, toxic side effects and the development of resistance and subsequent tumor relapse are frequently seen.

Therapeutic manipulation of the immune system has now emerged as an alternative approach to anti-cancer therapy, as a consequence of the development of inhibitors targeting the immune checkpoint proteins PD-1, PD-L1, and CTLA4 (2). Certain tumor types show impressive clinical responses to these agents, particularly melanoma (3), non-small cell lung cancer (4,5), and microsatellite instability (MSI)-high colon cancer (6,7). However, the majority of patients with most common tumor types, including breast cancer (8,9), ovarian cancer (10,11), and microsatellite-stable (MSS) colon cancer (12) show much lower response rates. It has been estimated that the overall percentage of all cancer patients who will respond to immune checkpoint inhibitors alone is less than 13% (13).

For many tumor types, immunotherapy has been reserved as a second- or third-line treatment option in patients who have failed prior treatment with cytotoxic agents (14). However, early combination treatment using chemotherapy and immune checkpoint inhibitors as a first line therapeutic modality was recently approved for advanced non-small cell lung cancers (NSCLC) that lack epidermal growth factor (EGFR) or anaplastic lymphoma kinase (ALK) mutations using cisplatin and pembrolizumab (15), for head and neck squamous cell carcinomas (HNSCC) using platinum agents, 5-fluorouracil (5-FU), and pembrolizumab (16), and for triple negative breast cancer (TNBC) using pembrolizumab and either paclitaxel or gemcitabine plus carboplatin (17).

Data supporting this approach comes from the KEYNOTE-189 trial, which showed a median progression-free survival of 8.8 months in patients with NSCLC that were treated with a combination of cisplatin or carboplatin, pemetrexed, and pembrolizumab, compared

to 4.9 months in patients who were treated with chemotherapy alone. However, over 65% of the patients who received this chemotherapy and immunotherapy combination continued to have progressive disease (15). Similarly, the KEYNOTE-048 trial, performed in patients with recurrent unresectable HNSCC in which the tumor contained greater than 1% of cells staining positively for PD-L1, failed to show any improvement in progression-free survival in patients treated with cisplatin or carboplatin, 5-FU, and pembrolizumab, compared to those treated with the same chemotherapy plus cetuximab, although there was an increase in median overall survival from 10.7 months to 13 months when pembrolizumab was included in the combination (16). Finally, in the KEYNOTE-355 trial involving patients with locally recurrent but inoperable or metastatic TNBC, the median progression-free survival at 12-months in patients whose tumors showed ≥ 10% PD-L1–positive staining increased from 23% to 39% by the addition of immunotherapy to chemotherapy compared with chemotherapy alone, but over 70% of the intention-to-treat population had progressive disease by this time (17). Identifying mechanisms that would enhance response rates to the combination of immune checkpoint blockade and chemotherapy—and prolong the durability of the response—remains an unmet clinical need.

Based on our long-standing interest in cross-talk between the DNA damage response and signaling pathways that mediate tumor cell survival, apoptotic cell death, and innate immune activation (18-23), we investigated whether signaling pathways activated in response to specific types of DNA damaging chemotherapy could enhance subsequent anti-tumor immune responses. Although the ability of specific chemotherapeutic compounds to enhance cross presentation of tumor antigens by dendritic cells has been characterized as “immunogenic cell death” (24-27), we found that chemotherapy-induced cell stress signaling in live injured cells, but not the presence of dead cells, was the primary determinant of T cell immunity. This effect is mediated by DNA-dependent protein kinase (DNA-PK), ataxia telangiectasia and Rad3-related kinase (ATR), nuclear factor κB (NF-κB), p38 mitogen-activated protein kinase (p38 MAPK) and receptor-interacting Ser/Thr kinase 1 (RIPK1) signaling in the injured tumor cells, depending on the drug and cell type. Furthermore, we show that direct intra-tumoral injection of ex vivo chemotherapy-treated cells as an injured cell adjuvant, in combination with systemic immune checkpoint blockade drives anti-tumor immunity and tumor regression in murine melanoma models, in contrast to immune checkpoint blockade alone.

## RESULTS

### Etoposide and mitoxantrone-treated tumor cells can induce DC-mediated OT-I T-cell IFN-γ responses in vitro

To identify how tumor cell stress and injury after DNA-damaging chemotherapy could potentially influence anti-tumor immune function, we treated B16F10 melanoma tumor cells expressing ovalbumin (B16-Ova), or MC-38 colon cancer cells expressing ovalbumin (MC38-Ova; fig. S1A) with various doses of the common clinically used chemotherapeutic agents doxorubicin, etoposide, mitoxantrone, cisplatin, oxaliplatin, cyclophosphamide, irinotecan, camptothecin, paclitaxel or 5-FU, and examined them for immunogenicity by assaying for their ability to induce dendritic cell-mediated IFN-γ responses in $CD8^+$ T cells.

After tumor cell treatment with chemotherapeutic drugs for 24 hours, the drugs were washed out with two or more changes of media, and the treated cell mixture (including both injured and dead cells) was then co-cultured with primary bone-marrow derived dendritic cells for an additional 24 hours (Fig. 1A). Purified naïve $CD8^+$ T cells obtained from the spleens of OT-1 mice were then added to the drug-treated B16-Ova cells/BMDC co-culture, and the appearance of IFN-$\gamma^+$ $CD8^+$ T cells was quantified 12 to 15 hours later by intracellular staining and flow cytometry (Fig. 1B). $CD8^+$ T cells of OT-1 mice express a transgenic T-cell receptor recognizing ovalbumin residues 257-264 in the context of H2-$K^b$ (31,32).

Treatment of B16-Ova or MC38-Ova cells with either etoposide or mitoxantrone was the most effective at inducing DC-mediated IFN-γ in OT-1 $CD8^+$ T cells when the treated cells were co-cultured with BMDCs (Fig. 1, C and D, and fig. S1B). The effectiveness of these DNA-damaging drugs at inducing T cell IFN-γ responses was dose-dependent for each cell line. Unexpectedly, in contrast to etoposide and mitoxantrone (both DNA topoisomerase II inhibitors), doxorubicin (also a topoisomerase-II inhibitor but in a different drug class, anthracyclenes) was ineffective at inducing DC-mediated IFN-γ in T cells when administered at comparable doses, despite causing similar or higher levels of total cell death (Fig. 1, C and D, and fig. S1, C and D). The effects of 50 μM etoposide, 10 μM mitoxantrone and 10 μM doxorubicin on T cell stimulation assayed by IFN-γ production was consistent with the effects of these drugs on T cell proliferation, as assayed by carboxifluorescein diacetate succinimidyl ester (CFSE) dilution (fig. S1E).

To examine whether the anti-tumor immune response induced by chemotherapy treatment required the artificial expression of ovalbumin and the OT-1 T cell system, we used a second tumor cell line, TC-1, which was previously established from mouse lung tumors by immortalization with human papilloma virus (HPV) protein E7 (33). To generate T cells specific for the E7 antigen, mice were vaccinated with three doses of an HPV E7 peptide, and total splenic $CD8^+$ T cells were isolated 6 days after the third immunization. This bulk population of splenic T cells was then used in drug treatment experiments with TC-1 cells, as described above (for Fig. 1E). Similar to what was seen in the MC-38-Ova/OT-1 experiments, TC-1 cells treated with the indicated doses of etoposide and mitoxantrone, but not with similar doses of doxorubicin, showed an enhanced IFN-γ response (Fig. 1F), with the strongest response to mitoxantrone at 50 μM.

## Conventional markers of immunogenic cell death do not fully explain the T-cell response to mitoxantrone and etoposide treatment.

In our in vitro assay system, both mitoxantrone and etoposide were found to induce dendritic cell-mediated T cell IFN-γ responses, in contrast to doxorubicin (at 10 and 50 μM). Obeid *et al.* (24) reported that mitoxantrone chemotherapy induced strong immunogenic cancer cell death in CT26 mouse colon carcinoma cells, based on the drug's ability to induce calreticulin exposure on the cell surface. Prophylactic subcutaneous injection of these dying, drug-treated cells into one flank enabled mice to resist a subsequent tumor challenge into the opposite flank (24). In addition to externalized calreticulin, release of high mobility group box protein 1 (HMGB1) and adenosine triphosphate (ATP) were also reported to serve as canonical markers of immunogenic cell death (27).

To directly test whether these markers correlated with T cell priming in our system, we treated B16-Ova cells with mitoxantrone, etoposide, or doxorubicin and measured calreticulin exposure on the cell surface at 24 hours, when the treated cells were cultured with BMDCs. We also analyzed HMGB1 and ATP release during the first 24 hours of chemotherapy treatment and during the 24- to 48-hour post-treatment window, which corresponds to the full period of BMDC co-culture (Fig. 2A). In previous reports, etoposide was not considered an immunogenic cell death-inducing drug due to its inability to induce endoplasmic reticulum (ER) stress and calreticulin exposure in CT26 cells (24), despite inducing the release of HMGB1 and ATP (34). However, we included etoposide in these experiments because it induced equivalent levels of IFN-$\gamma^+$CD8$^+$ T cells as mitoxantrone in our in vitro assay for DC-mediated T cell responses. Doxorubicin was specifically chosen as the third drug for comparison because, like etoposide and mitoxantrone, it inhibits topoisomerase II, but did not induce T cell IFN-γ responses when used at similar doses (Fig. 1, B and C), although this has been reported to induce calreticulin exposure and the release of HMGB1 and ATP in CT26 cells (24,34).

Using two calreticulin antibodies, all three drugs elicited only low levels of calreticulin exposure at this time point (24 hours), with <20% of the cells staining positively (Fig. 2A and fig. S2A, left panels). Mitoxantrone-treatment induced the highest percentage of cells with externalized calreticulin when analyzed by flow cytometry after 24 hours of drug exposure. Treatment with either low or high etoposide concentrations caused an intermediate percentage of cells to display calreticulin surface exposure (<10%), whereas doxorubicin treatment resulted in the lowest percentage of cells with calreticulin exposure (<5%).

There was no correlation between HMGB1 or ATP release and induction of immunogenicity as measured by IFN-γ production in stimulated T cells (Fig. 2A, middle and right panels). Cells treated with etoposide showed the lowest levels of HMGB1 release into the media during the 24- to 48-hour post-treatment window (meaning, when the tumor cells were exposed to BMDCs; Fig. 2A, middle panel), despite being highly immunogenic. In contrast, but similar to what was observed with mitoxantrone (10 μM) treatment, doxorubicin treatment led to high levels of HMGB1 release, despite its inability to promote BMDC-mediated T cell IFN-γ responses at this dose. Similar trends in HMGB1 release were observed during the first 24 hours of treatment (fig. S2B). During the first 24 hours of drug exposure, ATP release from B16-Ova cells following doxorubicin and mitoxantrone treatment but not etoposide treatment was higher than the control (fig. S2C), despite the observation that only mitoxantrone and etoposide-treated B16-Ova cells induced DC-mediated IFN-γ in T cells. Levels of ATP release following etoposide treatment of B16-Ova cells were not statistically significantly different than those levels of ATP released by DMSO-treated controls (fig. S2C). During the 24- to 48-hour window after drug exposure, when B16-Ova cells are co-cultured with BMDC, the release of ATP by B16-Ova cells for all drug/dose treatment conditions was comparable to the baseline levels induced by the vehicle control condition (Fig. 2A, right panel). Overall, whereas the calreticulin exposure on the total treated cell mixture partially explains the differences in chemotherapy-induced tumor cell immunogenicity, neither HMGB1 release nor ATP secretion were predictive of DC-mediated T cell IFN-γ responses for all three chemotherapy agents.

Given the lack of correlation between HMGB1 or ATP release from the drug-treated tumor cells and dose-specific induction of IFNγ in T cells, we focused on the specific role of calreticulin. To directly measure the contribution of calreticulin to DC-mediated T cell IFN-γ responses in our assay, the experiments outlined above (in Fig. 1A) were repeated after knockdown of calreticulin in B16-Ova cells using targeted small interfering RNA (siRNA) (Fig. 2B). Knockdown of calreticulin prior to drug treatment reduced the percentage of DC-mediated IFN-$\gamma^+$ T cells after mitoxantrone exposure by ~80% and the percentage of DC-mediated IFN-$\gamma^+$ T cells after etoposide exposure by ~50% (Fig. 2C). These data suggest that in B16-Ova cells, calreticulin can account for a substantial amount of the drug-induced anti-tumor immunogenicity, consistent with its previously described role in immunogenic cell death (24). However, two other previously described canonical markers of immunogenic cell death, HMGB1 and ATP, failed to explain the observed results.

## T cell IFN-γ responses by BMDC co-cultured with DNA-damaged tumor cells depends on RIPK1, NF-κB, and p38 MAPK signaling in the tumor cells

To further explore the signaling connection between anti-tumor immunogenicity and cell death, we inhibited the kinase RIPK1, which is a known determinant of necroptosis (35), caspases, which are known determinants of apoptosis and pyroptosis (36), the transcription factor NF-κB, which is a critical regulatory node for survival and cytokine production (37), and the kinase p38 MAPK, which is a well-known master regulator of stress signaling, including signaling downstream of DNA damage (38), all of which were activated by etoposide and/or mitoxantrone treatment (fig. S2, D to G). B16-Ova cells were co-treated with etoposide or mitoxantrone in combination with the RIPK1 inhibitor necrostatin-1 (Nec-1), the pan-caspase inhibitor Z-VAD, the NF-κB signaling inhibitor Bay 11-7085 (39) or the p38 MAPK inhibitor SB202190 (40), and the drugs were washed out prior to co-culture with BMDC. Co-treatment with Nec-1 inhibited the ability of both etoposide and mitoxantrone-treated, B16-Ova cells, co-cultured with BMDCs, to induce IFN-γ in T cells (Fig. 2, D and E), suggesting that the ability of both etoposide and mitoxantrone to induce immunogenicity in this model is RIPK1-dependent. In contrast, co-treatment of B16-Ova cells with Z-VAD (validated in fig. S2D) only marginally reduced T cell IFN-γ responses (by ~12%) with etoposide and had no effect with mitoxantrone, indicating that the process for both agents was largely independent of caspases. Furthermore, co-treatment of B16-Ova cells with the NF-κB signaling inhibitor Bay 11-7085 (validated in fig. S2E) and etoposide reduced the frequency of IFN-$\gamma^+$ T cells by >90%, whereas co-treatment with Bay 11-7085 and mitoxantrone reduced the frequency of IFN-$\gamma^+$ T-cells by >50%, suggesting that NF-κB signaling in both etoposide and mitoxantrone-treated B16-Ova cells is important for the induction of DC-mediated T cell IFN-γ responses. Finally, co-treatment of B16-Ova cells with the p38 MAPK inhibitor SB202190 and etoposide reduced the frequency of IFN-$\gamma^+$ T cells by ~22%, whereas co-treatment with SB202190 and mitoxantrone nearly abrogated the induction of IFN-$\gamma^+$ T cells altogether. Consistent with these results, both etoposide and mitoxantrone (which induced DC-mediated T cell IFN-γ responses) but not doxorubicin (which did not) were found to induce RIPK1 activation in B16-Ova cells, as shown by Western blotting with an antibody to $Ser^{166}$-phoshorylated RIPK1 (fig. S2F). Western blotting of cell lysates with an antibody to phosphorylated p38 demonstrated p38 MAPK activation by etoposide and mitoxantrone, as well as by doxorubicin, suggesting

that induction of p38 MAPK signaling in tumor cells is necessary but not sufficient for the induction of IFN-γ in T cells (fig. S2G). Together, these data suggest that active signaling through the RIPK1, NF-κB and p38 MAPK signaling pathways following chemotherapy treatment is involved in the induction of DC-mediated T cell IFN-γ responses. Similar results were obtained in MC-38-Ova cells for all but RIPK1, the inhibition of which in etoposide-treated tumor cells had minimal effects on T cell IFN-γ production and actually enhanced its production in response to mitoxantrone-treated tumor cells (Fig. 2, F and G).

## In situ treatment of B16-Ova tumors with direct intra-tumoral etoposide does not synergize with systemic checkpoint blockade, consistent with immune cell damage

Given the wide clinical use of etoposide in oncology (41), and the ability of etoposide-treated B16-Ova cells to induce DC-mediated T cell IFN-γ responses ex vivo, as presented above (Fig. 1), we reasoned that intra-tumoral administration of etoposide could enhance DC function in vivo by increasing the immunogenicity of B16-Ova cells. This would be expected to induce antigen-specific T-cell expansion in vivo, particularly if used in combination with systemic immune checkpoint blockade. To test this, mice bearing flank B16-Ova tumors were treated by intra-tumoral administration of either saline or etoposide (three weekly doses) in the presence or absence of systemic anti-PD1 and anti-CTLA4 antibodies (two doses a week for three weeks) to confer immune checkpoint blockade (Fig. 3A). Intra-tumoral injection of etoposide alone had no effect on tumor growth (Fig. 3B, upper panels). Systemic administration of immune checkpoint blockade in combination with intra-tumoral chemotherapy also did not significantly enhance survival beyond that seen with immune checkpoint blockade alone (Fig. 3, B and C). Furthermore, when we examined the frequency of circulating H2-$K^b$/SIINFEKL–specific $CD8^+$ T cells, we were unable to detect an expansion of these cells when compared to the group that received checkpoint blockade alone (Fig. 3D).

However, intra-tumoral administration of etoposide exposes both tumor cells and non-tumor cell types such as intra-tumoral DCs to this cytotoxic drug, which could potentially limit DC activation and impair the expansion of tumor antigen-specific T-cells. To test this hypothesis, we revised the assay described above (shown in Fig. 1A) to now include co-exposure of tumor cells and either BMDCs or both BMDCs and T cells to etoposide prior to the addition of OT-1 T-cells (Fig. 3E and fig. S3A). Co-exposure of both BMDCs and tumor cells to etoposide significantly reduced the appearance of IFN-$\gamma^+CD8^+$ T cells compared to exposure of B16-Ova cells alone (fig. S3A), indicating that exposure of DCs to etoposide impairs their ability to induce T cell IFN-γ responses. Consistent with this idea, the viability of BMDCs was significantly reduced upon exposure to etoposide (fig. S3B). We further modified the assay to include exposure of all of the relevant cell types—tumor cells, BMDCs, and T cells—to etoposide, mirroring what might occur following intra-tumoral injection of the drug in vivo. This triple co-exposure resulted in an even more profound loss of IFN-γ+ T-cells to less than 10% of the level seen when etoposide exposure is limited to the tumor cells alone (Fig. 3F).

### *Intra-tumoral injection of* ex vivo *etoposide-treated tumor cells synergizes with immune checkpoint blockade to enhance the anti-tumor response and survival*

Exposure of BMDC and T-cells to etoposide reduced the induction of IFN-$\gamma^+$CD8$^+$ T-cells by drug-treated B16-Ova cells compared to etoposide exposure of B16-Ova cells alone. We therefore reasoned that the intra-tumoral injection of ex vivo etoposide-treated B16-Ova cells into B16-Ova tumors in vivo, rather than intra-tumoral injection of the free drug, would minimize exposure of other immune cell types in the tumor and draining lymph node to the cytotoxic effects of etoposide. To test this, mice bearing flank B16-Ova tumors received intra-tumoral injection of either saline or ex vivo etoposide-treated B16-Ova cells in the presence or absence of systemic checkpoint blockade (Fig. 4A). Intra-tumoral administration of ex vivo etoposide-treated tumor cells alone had no effect on subsequent tumor progression (Fig. 4, B to D). However, when used in combination with systemic checkpoint blockade, the mice displayed superior tumor control compared to those that received checkpoint blockade alone, resulting in complete tumor regressions in ~35% of mice. Furthermore, survival was also markedly enhanced in this group (Fig. 4C). Notably, analysis of circulating lymphocytes in these animals revealed an enhanced frequency of H2-K$^b$/SIINFEKL-specific CD8$^+$ T-cells (Fig. 4E), indicating that intra-tumoral administration of ex vivo etoposide-treated tumor cells functions as an effective injured cell adjuvant, which in combination with immune checkpoint blockade, promotes efficient T-cell priming and anti-tumor immunity.

To test if the site of injection of the injured cell adjuvant was critical for the subsequent anti-tumor response in combination with checkpoint blockade, we compared direct intra-tumoral injection with a distant site subcutaneous injection draining into the axillary lymph node in the opposite flank (Fig. 4F). Mice that received intra-tumoral injections showed superior tumor control, survival, and cure compared to animals that received subcutaneous injections draining into the axillary lymph node in the opposite flank from that bearing the primary tumor (Fig. 4G).

### Intra-tumoral injection of ex vivo etoposide-treated tumor cells results in persistent cure and immunological anti-tumor memory in a subset of treated mice

The subset of mice that demonstrated complete tumor regression after injured cell adjuvant treatment remained tumor-free for at least 98 days (Fig. 4C). These complete responders and naive control mice (which were never previously exposed to B16-Ova tumor cells) were re-challenged in the contralateral flank with live B16-Ova cells (Fig. 5A, supper panel). Tumors grew to 200 mm$^2$ cross-sectional area within 30 days in the naive mice (Fig. 5A, lower panel), at which point they were euthanized. Notably, none of the intra-tumoral adjuvant-treated animals who were cured of their initial tumors after therapy developed tumors upon re-challenge, suggesting that combining systemic checkpoint blockade with intra-tumoral injections of the injured cell adjuvant induces anti-tumor immunological memory.

To examine whether this response was unique to the B16 cell line, or to cells engineered to express the ovalbumin antigen, we performed similar intra-tumoral injections of saline- or etoposide-treated tumor cells, in the presence or absence of systemic immune checkpoint

blockade, with MC-38 murine colon carcinoma cells that do not express ovalbumin (fig. S4A). In this MC-38 tumor model, there was minimal benefit of immune checkpoint blockade alone when the tumors were injected with saline (fig. S4, A and B). Similarly, direct intra-tumoral injection of etoposide-treated MC-38 tumor cells into pre-existing MC-38 tumors failed to elicit an anti-tumor immune response in the absence of systemic immune checkpoint blockade. However, 20% of the animals who received the combination of the etoposide-treated MC-38 tumor cells together with systemic immune checkpoint blockade showed complete tumor regression and prolonged survival.

Finally, to evaluate whether T-cell responses were being elicited towards non-ovalbumin endogenously expressed tumor antigens in the B16-Ova model, mice that showed complete tumor regression were re-challenged with live B16-Ova cells and sacrificed 6 days later. The spleens were harvested, and the splenocytes then re-stimulated in vitro with either B16-OVA cells, the parental B16F10 cell line that does not express ovalbumin, or with the SIINFEKL peptide, and the number of IFN-γ producing cells was examined using an ELISPOT assay. All three re-stimulation conditions resulted in the appearance of IFN-γ positive cells, whereas no such cells were seen in the spleens of naïve mice that had not been previously inoculated with B16-Ova cells (Fig. 5B). Notably, the appearance of IFN-γ positive cells upon restimulation with B16F10 cells lacking ovalbumin expression indicates that T cells in the cured mice can recognize endogenously expressed tumor antigens in addition to the artificially expressed ovalbumin protein.

## Batf3$^{-/-}$ mice do not respond to the injured cell adjuvant and checkpoint blockade combination

To test whether the efficacy of the injured cell adjuvant in combination with immune checkpoint blockade treatment for an anti-tumor immune response depends on DCs that can cross-present tumor antigens, we enumerated the numbers of CD11b$^{+}$C103$^{-}$ DC2 cells and CD11b$^{-}$CD103$^{+}$ DC1 cells by immunophenotyping and flow cytometry (fig. S5A). CD11b$^{-}$CD103$^{+}$ DC1 cells, which are typically also BATF3$^{+}$ (42,43), are known to cross-present tumor antigens to CD8$^{+}$ T cells (44). As above, flank-implanted B16-Ova tumors were injected directly with saline or the etoposide-treated injured cell adjuvant in the presence or absence of systemic checkpoint blockade (Fig. 6A). We also included a cohort of mice that was treated with intra-tumoral etoposide in combination with checkpoint blockade. After two doses of the injured cell adjuvant or etoposide and three doses of checkpoint blockade, immunophenotyping of the tumors revealed an enhanced number of CD103$^{+}$ DC1 in tumors that were treated with the injured cell adjuvant and checkpoint blockade, compared to the other groups (Fig. 6B). In addition, cross-sections of tumors treated with the injured cell adjuvant and checkpoint blockade showed markedly enhanced BATF3 staining by immunohistochemistry (Fig. 6C), indicating the enhanced presence of BATF3$^{+}$ DCs, which was not present in the other treatment groups. Intra-tumoral injection of free etoposide combined with checkpoint blockade did not enhance numbers of CD103$^{+}$ DC1, consistent with the lack of T cell expansion and lack of efficacy seen in vivo (Fig. 3, A to D) and in vitro (Fig. 3F) with this treatment.

To directly validate the contribution of $BATF3^{+}CD11b^{-}CD103^{+}$ DC1 cells to anti-tumor immunity induced by the combination of our injured cell adjuvant and checkpoint blockade, the experiment above (Fig. 4A) was repeated using *Batf3*$^{-/-}$ mice. Intra-tumoral injection of ex vivo etoposide-treated tumor cells with systemic immune checkpoint blockade failed to induce tumor control or prolong the lifespan of tumor-bearing mice in the absence of BATF3 (Fig. 6, D and E). Lastly, whereas the combination of the injured cell adjuvant and systemic immune checkpoint blockade showed an enhanced trend in the frequency of circulating H2-$K^{b}$/SIINFEKL–reactive $CD8^{+}$ T cells in WT mice, this trend was not observed in BATF3-deficient mice (Fig. 6F).

To further explore the presence of co-stimulatory markers on DC1 cells, mice bearing B16-Ova tumors were treated with a single dose of saline or the etoposide-treated injured cell adjuvant intra-tumorally, in the presence or absence of a single systemic dose of anti-PD1/anti-CTLA4 antibodies given 24 hours previously. The tumors were then harvested 24 hours later, disaggregated, stained for markers of DC1, the costimulation molecules CD86 and OX40L, and the chemokine receptor CCR7, and quantified by flow cytometry. The combination of intra-tumoral injection of etoposide-treated injured cells with systemic checkpoint blockade resulted in enhanced density of activated DC1 cells within the tumor as early as 24 hours after a single dose of the adjuvant (Fig. 6G and fig. S5B). Together, these data strongly suggest that intra-tumoral administration of ex vivo etoposide-treated tumor cells as an injured cell adjuvant, in combination with systemic checkpoint blockade, promotes $BATF3^{+}$ DC-mediated anti-tumor T cell responses leading to improved survival, and complete tumor regressions in a subset of mice concurrent with long-term anti-tumor immunological memory.

## Live injured cells, rather than dead cells, are the determinants of DC-mediated IFN-γ induction in T cells

We observed that both etoposide and mitoxantrone, which effectively induced DC-mediated IFN-γ in $CD8^{+}$ T cells, induced substantial amounts of apoptotic and non-apoptotic tumor cell death compared to drugs that failed to elicit an immune response (fig. S6A), Notably, doxorubicin also caused similar amounts of cell death but was immunologically silent. Curiously, at the drug doses used here (in fig. S6A), the specific doses of mitoxantrone and etoposide that were maximally effective were not the doses that caused the greatest amount of total cell death.

To investigate whether the magnitude of T cell IFN-γ responses directly correlated with the number of dead cells present in the treated tumor cell fractions that were co-incubated with BMDC, we treated tumor cells with increasing doses of etoposide or mitoxantrone from 0 to 100 μM. Using the assay described above (in Fig. 1A), B16-Ova cells treated with increasing doses of etoposide, induced a corresponding increase in the magnitude of IFN-γ responses in T cells (Fig. 7A). However, the proportion of dead cells (AnnV or DAPI single or double positive) present in the treated tumor cell mixture increased to ~ 30% at 25 μM etoposide, but was largely unchanged with greater doses; whereas cells treated with 5 μM mitoxantrone induced the maximum IFN-γ responses in T cells among the doses tested, and cells treated with 10 μM mitoxantrone induced a lower IFN-γ response that became undetectable at 25

μM and greater doses (Fig. 7, B and C). The dead-cell proportion in the mitoxantrone-treated B16-Ova cell mixture was equivalent between 5 and 10 μM (~ 50%) and increases to greater than 90% at 25 μM and higher doses (Fig. 7D). These results indicated that there was no agreement between the proportion of dead cells induced by etoposide or mitoxantrone treatment and the DC-mediated IFN-γ responses in T cells, although all the doses that were immunologically active resulted in some degree of cell death, which was generally ≤~50%.

To further investigate the specific contribution of the dead and live fractions of tumor cells induced by chemotherapy treatment, we fractionated the etoposide- and mitoxantrone-treated cell cultures into cell-free supernatants, dead-cell-enriched fractions (AnnV+ and/or DAPI+), or live-cell-enriched fractions (AnnV and DAPI double negative) (fig. S6, B to E). Each fraction was then co-cultured with BMDCs for 24 hours, followed by the addition of OT-1 $CD8^+$ T cells for an additional 12 to 15 hours, as described above (for Fig. 1A). Neither the cell-free supernatants nor the dead cell-enriched fraction, alone or in combination, was capable of inducing DC-mediated T cell IFN-γ responses (Fig. 7, E to H). Furthermore, consistent with the finding that cell-free supernatants alone did not induce T cell priming for IFN-γ production, analysis of the cytokines in the supernatants after co-culture of chemotherapy-treated cells with DCs using a 44-cytokine panel revealed that no single cytokine was sufficiently changed to explain the differences observed between the immunogenicity of the different chemotherapy drugs used (fig. S7A). Co-treatment of tumor cells with brefeldin A in combination with etoposide or mitoxantrone resulted in only a small reduction in T cell IFN-γ production by the etoposide-treated tumor cells and no reduction with mitoxantrone treatment (fig. S7B), suggesting that active secretion of factors from drug-treated tumor cells plays, at most, a limited role. Lysates generated by subjecting the chemotherapy-treated total cell mixture to three rounds of freeze-thawing (between liquid nitrogen and 37°C), upon co-incubation with BMDC, also failed to induce IFN-γ in T cells. In marked contrast, fractions containing the adherent live injured cells were the most effective at inducing the expression of IFNγ in OT-1 T-cells. Similar behavior was also noted in the MC-38-Ova cells (Fig. 7, G and H).

Finally, to directly verify these effects in vivo, we repeated above-described experiments (in Fig. 4A) in which mice bearing B16-Ova tumors were given intra-tumoral injections of either the live-injured cell fraction or the dead cell fraction of B16-Ova cells that had been treated ex vivo with 50μM etoposide, followed by systemic administration of α-PD1/CTLA4 immune checkpoint inhibitors (Fig. 7I). Two days after the second intra-tumoral dose of the live injured or the dead cell fractions, mice were sacrificed, and the percentage of H2-$K^b$-SINFEKL–specific T cells within the tumor were enumerated using flow cytometry. Only intra-tumoral injection of the live injured cell fraction after chemotherapy treatment resulted in significant tumor-specific T cell infiltration in vivo (Fig. 7J).

We were perplexed by the failure of the 10 μM or 50 μM doxorubicin treatments to induce an effective immunogenic response in our assay, because this drug has previously reported to be capable of inducing anti-tumor immunity in vivo (24,45). We therefore repeated these DC-mediated T cell stimulation assays after treatment of the B16-Ova tumor cells with lower doses of doxorubicin. When the doxorubicin dose was reduced, substantial IFNγ production could be observed, with a maximal effect seen at 1 μM (Fig. 8A). Consistent with

what we observed with 50 μM etoposide and 10 μM mitoxantrone, treatment of the B16-Ova cells with 1 μM doxorubicin also resulted in substantial DC-mediated T cell proliferation (fig. S1E), in contrast to what we had observed with the 10 μM dose.

### DNA damage signaling in the live-cell fraction is critical for the T cell IFN-γ response.

To further investigate the role of DNA damage signaling in the immunogenicity induced by chemotherapy treatment in the live-cell fraction, we performed immunofluorescence microscopy and validated that treatment with the maximally effective doses of doxorubicin, etopiside, and mitoxantrone resulted in intense γH2AX nuclear foci formation in the live B16-Ova tumor cells (Fig. 8, B and C). Next, a total population of drug treated cells was separated into live and dead cell fractions, and lysates of each fraction were immunoblotted using phospho-specific antibodies directed at the phospho-SQ motif present on substrates of the DNA damage kinases ATM, ATR, and DNA-PK (46). The extent of DNA damage signaling was clearly more pronounced in the injured live cell fraction (Fig. 8D). Finally, to investigate the extent to which this DNA damage signaling contributed to the immunogenicity phenotype, the cells were treated with small molecule inhibitors of ATM, ATR, or DNA-PK prior to treatment with 50 μM of etoposide and assayed for DC-mediated T cell production of IFNγ (as described above in Fig. 1A). Pre-treatment with the DNA-PK inhibitor was particularly effective in suppressing DC-mediated T cell stimulation after chemotherapy treatment, with modest effects also seen following ATR inhibition (Fig. 8E). Some reduction in production was also observed upon ATM inhibition, though this failed to reach statistical significance. The effect was independent of direct sensing of cytosolic DNA by BMDCs, since *Sting*$^{-/-}$ BMDCs were equally effective in inducing T cell responses by DNA-damaged tumor cells (fig. S7C). Together with the results showing that the immunogenicity resided in the live cells (Fig. 7), these data indicate that DNA damage signaling within the live, injured cell fraction after treatment with genotoxic drugs is critical for the development of effective anti-tumor T cell responses.

## DISCUSSION

The property of certain chemotherapeutic agents to activate the immune response has classically been attributed to their ability to induce immunogenic cell death in cancer cells, as reflected by multiple markers including calreticulin, HMGB1, and ATP (24,45,47,48). Separately, necroptotic death driven by RIPK3 in tumor cells has been shown to be effective in inducing an anti-tumor CD8+ T cell response (49,50). Finally, elegant work from Steve Tait's group using BH3 mimetics has implicated caspase-independent cell death by Mitochondrial Outer Membrane Permeabilization (MOMP) in engaging potent anti-tumor immune responses (51,52). Each of these studies clearly indicates the ability of specific types of cell death to stimulate an immune response, but the role of live stressed and injured cells, rather than dead cells, in promoting immune activation is not clear.

In this study, we used a novel adaptation of an antigen cross-presentation assay (53) to identify specific drug- and dose-dependent DNA-damaging conditions, and observed that live genotoxically injured tumor cells, when co-cultured with BMDCs, could drive T cell activation. Administration of ex vivo chemotherapy-treated live injured tumor cells

directly into a pre-existing tumor in vivo functioned as a potent immune adjuvant when given in combination with systemic ICB in mouse cancer models. This treatment led an expansion of $CD103^+$ intra-tumoral DCs, and an increase in the frequency of H2-$K^b$/SIINFEKL-reactive anti-tumor $CD8^+$ T cells in the tumor and in the circulation, resulting in markedly enhanced tumor control and survival compared to injection of an injured cell adjuvant into the contralateral flank in combination with ICB, or by ICB alone. A subset of mice showed complete tumor regressions and resistance to re-challenge with live tumor cells, demonstrating immunological memory. A similar complete regression response was observed using MC-38 cells lacking ovalbumin, indicating that the results were not limited to one tumor cell type, or to cells that express a foreign non-tumor antigen. The findings are summarized in a model figure (Fig. 9).

The most effective drugs at inducing this BMDC-mediated T-cell IFN-γ response were topoisomerase II inhibitors when used at doses that induced some degree of cell death, though the immunogenic activity clearly resided in the live injured cell fraction. While calreticulin appeared to play an important role, neither the release of HMGB1 or ATP from damaged or dead cells appeared to be involved, suggesting that the immunogenic determinants in tumor cells following genotoxic stress reside within or on the surface of the injured cells. The function of calreticulin in the injured tumor cells awaits further clarification, but could involve mechanisms distinct from its effects on dead cell uptake by DCs (24), possibly involving its ER-chaperone activity (54-56). We cannot, however, completely exclude a contribution from chemotherapy-induced tumor cell death, given that some of the live injured cells after chemotherapy treatment may die during the co-incubation period with BMDCs.

Both DNA damage signaling and activation of the NF-κB pathway in the live injured tumor cells was critical for inducing anti-tumor immunogenicity. DNA damage signaling is known to activate NF-κB and contributes to survival of tumor cells after treatment with DNA damaging drugs (57-60). This process involves IKKγ (NEMO) nuclear import and export, and activation of IκB kinase which also involves RIP kinase 1 (RIP1) and the p38 MAPK kinase kinase TAK1 in a cytosolic complex (57), consistent with our findings of important roles for p38 MAPK and RIPK1. Our findings that p38 MAPK was more critical for mitoxantrone-induced immunogenicity, and that RIPK1 signaling played a critical role in B16-Ova cells but not MC-38-Ova cells suggests that other protein complexes may be involved in engaging NF-kB in a drug- and cell-type dependent manner. Activation of NF-kB has been extensively studied previously in the context of tumor cell resistance to anti-cancer therapies, but in light of our results implicating live injured cells in the T-cell IFN-γ response, this process may also be a physiological mechanism for cells to become immunogenic after DNA damage. Exactly how the activation of the DNA damage responsive PI-3 kinase-like kinases ATM, ATR, and DNA-PK, as well as p38 MAPK and NF-kB contribute to the immunogenicity of the live injured cells remains to be clarified in future work, but could involve, for example, upregulation of antigenic determinants on the tumor cells themselves (61).

Despite the known importance of RIPK1 activity in promoting non-apoptotic cell death (62,63), we did not observe significant amounts of necroptotic cell death. In this regard, our

findings complement those of Yatim *et al.* (49) and Snyder *et al.* (50) who independently showed a RIPK1-dependent but necroptosis-independent effect on the $CD8^+$ T cell response. In those experiments, Yatim *et al.*, found that artificial induction of RIPK3 in NIH-3T3 cells, followed by intradermal injection, induced priming of $CD8^+$ T-cells in vivo in a DC-dependent manner that required RIPK1 activity in the RIPK3-induced cells. In addition, NF-kB activity was also required. Snyder *et al.*, reported that overexpression of a synthetic RIPK3 dimerization construct in NIH-3T3 and B16 tumor cells in vitro, followed by intra-tumoral administration of these cells conferred significant tumor control and anti-tumor immunity. Remarkably, transfection with a RIPK3 variant that is unable to activate RIPK1, but that is still able to cause necroptotic cell death, failed to confer $CD8^+$ T-cell expansion or tumor control, demonstrating the importance of a non-necroptotic RIPK1 activity in this process, consistent with our finding of a role for RIPK1 signaling in live genotoxically injured cells.

Our results are in good agreement with recent studies wherein a subset of intra-tumoral dendritic cells, characterized by their surface expression of CD103 in mice and BDCA-3 in humans, was identified as having unique capabilities of cross-presenting tumor-associated antigens to $CD8^+$ T cells and recruiting T cells to the tumor microenvironment through CXCL9 or CXCL10 (44,64,65). The levels of these DCs in the tumor microenvironment was shown to correlate with better overall survival in melanoma patients receiving immune checkpoint inhibitors (66), consistent with the importance of these cells in enhancing anti-tumor immune responses.

Our finding that chemotherapy-induced live injured cells rather than dead cells are the major determinant of DC-mediated T-cell anti-tumor responses is entirely consistent with many of the concepts embodied in the “danger model’ of stress-induced immune activation described by Polly Matzinger in the 1990s [reviewed in (67)]. The danger model postulated that the expression of co-stimulatory molecules on antigen-presenting cells can be triggered by “danger signals,” or “alarm signals,” released by the body’s own stressed and injured cells. Consistent with this model, our findings point towards the concept of “immunogenic cell injury” rather than immunogenic cell death, as being critical for promoting anti-tumor T-cell responses following DNA-damaging chemotherapy. Finally, our results suggest a potential method to translate these findings into clinical use. Tumor cells from patient tumor biopsies could be used together with primary patient-derived or allogeneic DC and $CD8^+$ T cells to screen for the optimal chemotherapeutic compounds and doses that induce an immunogenic cell injury response. These injured cells could then be re-injected into the same tumor in combination with systemic checkpoint blockade. While clinical trials will be required to test efficacy, this approach has potential for patients whose cancers are accessible for intra-tumoral delivery and in whom conventional treatment options have failed and initial or acquired resistance to ICB has been observed.

## MATERIALS AND METHODS

### Reagents, cell lines, and mouse strains

Mouse GM-CSF and AnnV-FITC were purchased from BioLegend. IL-4 was purchased from Thermo Fisher Scientific. Antibodies to CD3ε (FITC; 145-2C11), to CD8 (APC;

53-6.7), to IFNγ (PE; XMG1.2), to CD45 (BUV395; 30-F11), to CD24 (APC; M1/69), to Ly6C (BV605; AL-21), to F4/80 (BV711; BM8), to MHCII (PE-Cy7; M5/14.15.2), to CD11b (BV786; M1/70), to CD103 (BV421; 2E7), to CD86 (clone GL1) , to CCR7 (clone 4B12), and to OX40L (clone RM134L) were purchased from eBioscience or BioLegend. H2-$K^b$/SIINFEKL-tetramer (PE-conjugated) was purchased from MBL Life Science. Necrostatin-1 and Z-VAD were purchased from Invivogen. Bay 11-7085 and SB202190 were purchased from Sigma. KU-55933, AZD6738 and NU7441 were from SelleckChem. Doxorubicin, etoposide, mitoxantrone, cisplatin, paclitaxel, camptothecin, irinotecan, 5-FU, and cylcophosphamide were purchased from LC Laboratories or Sigma. Oxaliplatin was purchased from Tocris Biosciences. Brefeldin A was from BioLegend. An antibody against ovalbumin was purchased from Abcam (Cat # ab17293). Antibodies to $Ser^{166}$-phosphorylated RIPK1 (Cat # 31122S) and RIPK1 (Cat # 3493T) were purchased from Cell Signaling Technology. Antibodies to calreticulin were purchased from Invitrogen (Cat # PA3-900) and Cell Signaling Technology (Cat # 12238T). The phospho-(Ser/Thr) ATM/ATR substrate antibody was purchased from Cell Signaling Technology (Cat # 2851S). CellTiter-Glo was purchased from Promega. CountBright absolute counting beads for flow cytometry, ACK lysis buffer, Lipofectamine RNAiMax transfection reagent, LIVE/DEAD Fixable Aqua Dead Cell Stain kit, and the Cell Trace CFSE proliferation kit were purchased from Thermo Fisher Scientific. HMGB1 ELISA kit was purchased from IBL International. $CD8^+$ T cell isolation kit was from STEM cell technologies. Anti-PD1 (clone RMP1-14) and anti-CTLA4 (clone 9D9) were from BioXcell. Antibody to BATF3 was purchased from Abcam (#ab211304). Antibodies to γH2AX and cleaved-PARP were from Cell Signaling Technology. B16F10 cells and MC-38 cells were obtained from ATCC. B16F10 cells were engineered to stably express ovalbumin (B16-Ova cells), as described previously (28). MC-38 Ova cells were generated by transduction of MC-38 cells with pLVX-Ovalbumin-IRES-hygro, selection of stable expression clones using hygromycin, followed by isolation and expansion of single cell clones. Ovalbumin expression was verified by Western blotting (fig. S1A). pSIRV-NF-kB-eGFP was a gift from Peter Steinberger (Addgene plasmid # 118093; http://n2t.net/addgene:118093; RRID:Addgene_118093) (29). To create a B16-Ova NF-κB reporter line, 293T cells were initially transfected with pSIRV-[NF-KB-RE]-eGFP (and Gag-Pol to generate retrovirus containing supernatant which was then used to transduce B16-Ova cells. Calreticulin siRNA (silencer select ID # s63272) was purchased from Thermo Fisher Scientific. C57BL/6J WT, *Batf3*$^{-/-}$, *Sting*$^{-/-}$ and OT-1 mice were purchased from Jackson Laboratories.

## BMDC generation

Bone marrow was harvested from the femurs and tibias of C57BL/6 mice (Taconic Biosciences). The bone marrow was flushed out after nipping one end, and then centrifuged at 15,000 x g for 15s. Following one round of RBC lysis with ACK lysis buffer, cells were filtered through a 100μm filter to remove aggregates, re-suspended at 1 x $10^6$ cells/ml, and cultured on a 10 cm bacterial plate (12 million cells per plate) in Iscove's Modified Dulbecco's Medium (IMDM) containing 10% FBS with antibiotics, 20 ng/ml each of GM-CSF and IL-4 and 55 μM of β-mercaptoethanol. After 3 days, 75% of the media was replaced with fresh media containing growth factors. Dendritic cells, which were loosely adherent, were harvested by gentle pipetting on day 6 or 7 and used for the assay.

### In vitro cross-presentation assay

B16-Ova or MC-38 Ova cells were treated with various doses of chemotherapeutic drugs for 24 hours followed by extensive washing in Iscove′s modified Dulbecco′s medium (IMDM; 10%FBS with penicillin/streptomycin). Subsequently 1 x $10^6$ treated cells were co-cultured with 2.5 x $10^5$ BMDC per well of a 24-well plate for each condition tested. After 24 hours of co-culture, supernatants were removed from each well and the BMDC washed 2 to −3 times in T cell media (RPMI containing 10% FBS, 20 mM HEPES, 1mM sodium pyruvate, 55 μM β-mercaptoethanol, 2mM L-glutamine, non-essential amino acids, and antibiotics). $CD8^+$ OT-I T cells isolated from spleens of OT-I mice were then co-cultured with the BMDC at 125,000 T-cells per well to achieve a T cell-to-BMDC ratio of 0.5. Where indicated, BMDC and/or T cells were also exposed to chemotherapy drugs. After a 12- to 15-hour incubation, IFN-γ producing T cells were identified and quantified by intra-cellular cytokine staining and flow cytometry using a BD LSR II or Fortessa flow cytometer. Cells were first gated for CD3 expression, then re-gated for CD8 and IFNγ expression.

In some experiments, B16-Ova cells were co-treated with 20 μM of necrostatin-1 or Z-VAD or 10 μM each of SB202190, Bay 11-7085, KU-55933, AZD6738, or NU-7441 and either etoposide or mitoxantrone at 10 or 50 μM for 24 hours prior to performance of the above assay.

For the cross-presentation assay using TC-1 cells to detect expansion of HPV-E7-specific $CD8^+$ T cells, TC-1 cells were treated with various doses of chemotherapeutic drugs for 24 hours followed by extensive washing in IMDM (10%FBS with penicillin/streptomycin). Subsequently 1 x $10^6$ treated cells were co-cultured with 2.5 x $10^5$ BMDC per well of a 24-well plate for each condition tested. After 24 hours of co-culture, supernatants were removed from each well and the BMDC washed 2 to 3 times in T cell media as described above. To generate an antigen-specific T cell population, C57BL/6 mice were injected subcutaneously at the tail base with 5 nmol HPV-E7 peptide vaccine [IDGPAGQAEPD*RAHYNIVTF* RQIKIWFQNRR(Nle)KWKK] containing 25 μg of c-di-GMP (Invivogen) as an adjuvant. Primed mice received two booster injections, 14 and 28 days after the first injection, with the same vaccine formulation. $CD8^+$ T-cells from spleens of C57BL/6 mice primed and boosted with HPV-E7 peptide vaccine were then isolated on day 6 after the booster dose and then co-cultured with the BMDC at 125,000 T cells per well to achieve an effector-to-target ratio of 0.5. After a 12- to 15-hour incubation, IFN-γ producing T cells were identified and quantified by intra-cellular cytokine staining and flow cytometry using a BD LSR II or Fortessa flow cytometer.

### CFSE dilution assay

B16-Ova cells were treated with various doses of chemotherapeutic drugs for 24 hours followed by extensive washing in IMDM (10%FBS, P/S). Subsequently 1 x $10^6$ treated cells were co-cultured with 2.5 x $10^5$ BMDC per well of a 24-well plate for each condition tested. After 24 hours of co-culture, supernatants were removed from each well and the BMDC washed 2-3 times in T cell media. $CD8^+$ OT-I T cells were isolated from spleens of OT-I mice and labeled with CFSE according to the manufacturer's protocol. 125,000 labeled T cells per well were cultured with BMDC in the presence of 10ng/ml IL-2 to achieve an

effector to target ratio of 0.5. CFSE dilution was assessed by flow cytometric analysis of the sample on day 5.

### Cytokine analysis

B16-Ova cells were treated with various doses of chemotherapeutic drugs for 24 hours followed by extensive washing in IMDM (10%FBS with penicillin/streptomycin). Subsequently 1 x $10^6$ treated cells were co-cultured with 2.5 x $10^5$ BMDC per well of a 24-well plate for each condition tested. After 24 hours of co-culture, supernatants were removed from each well and sent to Eve Technologies Inc. for the 44-Plex cytokine/chemokine array (MD44).

### Fractionation of live and dead fractions from chemotherapy-treated cells

B16-Ova cells or MC-38-Ova cells were treated with various doses of chemotherapy (as indicated in fig. S6) for 24 hours after which the floating fraction of cells was transferred to a separate tube and washed with PBS (for AnnV/DAPI staining) or IMDM (for co-culture with BMDC). The attached fraction was rinsed 1X with PBS, detached using 5 mM EDTA (in PBS), washed with PBS or IMDM and transferred to a separate tube. Separately, cells treated with chemotherapy for 24 hours were re-plated at 1 million cells per well of a 24-well plate in 500 μl of IMDM (10%FBS; P/S). Cell-free supernatants were collected after a further 24 hours. Staining with AnnV and DAPI of the attached and floating fractions after chemotherapy treatment and fractionation revealed that the attached fraction is predominantly AnnV and DAPI double negative suggesting that the majority of cells in this fraction are live injured cells; on the other hand, the floating fraction (labeled as “suspension” in fig. S7) consists of cells that predominantly stain positive for AnnV and/or DAPI suggesting that the majority of cells in this fraction are dead cells. Lysate of the total chemotherapy-treated cell mixture was generated by three rounds of freeze-thawing by alternate incubations in liquid nitrogen and a 37°C water bath.

### Measurement of immunogenic cell death markers

For measurement of calreticulin surface exposure, B16-Ova cells were treated for 24 hours with various chemotherapy drugs. All attached and floating cells were harvested and washed in staining buffer (PBS containing 0.5% BSA) and incubated with anti-calreticulin antibodies for 1 hour on ice. Cells were washed once in staining buffer and then incubated with secondary AF488-conjugated secondary antibody for 1 hour at room temperature, washed again, re-suspended in staining buffer, and analyzed by flow cytometry.

For HMGB1 measurement in cell culture media, B16-Ova cells were treated for 24 hours with various chemotherapy drugs, media was collected, and floating cells removed by centrifugation at 250 x g for 5 min. Cell-free cell culture media was collected at this time for the 24-hour time point. For the 48-hour time point, the total cell fraction was collected after 24 hours of drug treatment, washed extensively and re-plated for a further 24 hours after which the cell-free cell culture media was collected. These samples were then analyzed by ELISA for HMGB1 according to the manufacturer’s protocol.

For measurement of ATP levels, cell-free culture media obtained as above was analyzed by CellTiter-Glo according to the manufacturer's protocol. Values were converted to ATP concentrations using a standard curve generated using pure ATP.

### Calreticulin siRNA assay

B16-Ova cells were transfected with calreticulin or control siRNA (30 nM final concentration) using Lipofectamine RNAiMax according to the manufacturer's protocol. 48 hours post-transfection, cells were used for the in vitro cross-presentation assay.

### Cell death and viability assays

For assessment of cell death, floating and attached cells were harvested after 24 or 48 hours of treatment with the indicated chemotherapeutic drugs. Attached cells were detached using 5mM EDTA in PBS. The recovered cells were centrifuged at 250 x g for 5 min, washed once in PBS containing 0.9 mM $Ca^{2+}$ and 0.5 mM $Mg^{2+}$ and then stained with AnnV-FITC for 15 min in Annexin-binding buffer at room temperature according to the manufacturer's protocol (Biolegend). Cells were co-stained with DAPI at a final concentration of 1 μg/ml for 2 min in Annexin binding buffer, brought to a final volume of 500 μl using PBS containing 0.9 mM $Ca^{2+}$ and 0.5 mM $Mg^{2+}$ and analyzed by flow cytometry.

For assays of survival, 15,000 cells were plated per well in a 96-well plate in 100 μl media with 5 replicates per condition. Wells along the four edges of the plate were not used. After cell attachment, the indicated drugs were added in an equal volume of media, and incubated for an additional 48 hours. The media was then removed and replaced with 100 μl of fresh media at room temperature. Following a 30-min incubation at room temperature, 50 μl of CellTiter-Glo reagent was added, followed by 2 minutes of gentle mixing. The plate was incubated at room temperature for an additional 10 min. 100 μl of supernatant was transferred to a 96-well white opaque plate and luminescence was read on a Tecan microplate reader. Values were normalized to those of DMSO-treated control cells.

### ELISPOT assay

Naïve mice (that were never injected with tumor cells) and mice that showed complete tumor regression after treatment with intra-tumoral injured cell adjuvant and systemic anti-PD1 and anti-CTLA4 antibodies were re-challenged with 100,000 B16-Ova cells ipsilateral to the prior injection. On day 6 after re-challenge, mice were euthanized and spleens were harvested. Following RBC lysis with ACK lysis buffer, splenocytes were seeded as the effector cell population at 0.5x10^6 cells per well into mouse IFN-γ ELISPOT plates (BD). Target B16F10 or B16-Ova cells were treated overnight with 500 U/mL mIFN-γ and then gamma-irradiated at 120 Gy. Irradiated tumor cells were co-cultured with splenocytes at 25,000 cells per well for a period of 24 hours in a 37°C/CO2 incubator. Plates were developed according to the manufacturer's protocol and scanned using a CTL-ImmunoSpot Plate Reader. Quality control of spot identification was performed using CTL ImmunoSpot Software by a blinded researcher.

### Immunofluorescence

Immunofluorescence was performed by seeding cells onto glass coverslips in 12-well plates and treated with chemotherapy drugs. After 24 hours, floating cells were removed and the attached cells were washed in PBS, and then fixed with a 4% paraformaldehyde solution for 20 min at room temperature. Cells were blocked in 16.6% goat serum, 0.3% Triton X-100, 20 mM sodium phosphate, and 0.45 M sodium chloride prior to incubation with primary antibody (anti-γH2AX) overnight followed by secondary antibodies conjugated with Alexa Fluor (Invitrogen). Coverslips were then mounted using ProLong Gold Antifade Mountant (Invitrogen P36934) and imaged on EVOS FL Auto Cell Imaging System (Invitrogen). CellProfiler 3.0.0 (developed by the Broad Institute of MIT and Harvard's Imaging Platform and available at http://www.cellprofiler.org) was used to quantify the integrated intensity of cells stained with γH2AX antibody. Each image was broken down into its component grayscale images for analysis using a CellProfiler pipeline. An illumination function module was utilized to uniformly reduce and smoothen background staining on the entire image set. Cell nuclei were defined as primary objects using the DAPI grayscale images. The integrated intensity within the primary objects was then quantified for γH2AX foci.

### Mouse studies

B16-Ova cells or MC-38 cells ($1 \times 10^6$) were implanted subcutaneously in the right flank of 7- to 8-week old female C57BL/6J WT or BATF3-deficient (*Batf3*$^{-/-}$) mice. After 11 to 13 days, tumors of an approximate 16 $mm^2$ median cross-sectional area were typically detectable by palpation. Mice with tumors were then binned into groups and injected intra-tumorally once a week for 3 weeks with 30 μl of either PBS, free etoposide to achieve a final concentration of 50 μM in the tumor volume, or $1 \times 10^6$ etoposide-treated cells (24 hours of drug treatment followed by extensive washing with PBS). Where indicated, groups also received intra-peritoneal injections of 200 μg each of anti-PD1 (clone RMP1-14, BioXCell) and anti-CTLA4 (clone 9D9, BioXcell) twice a week for three weeks. Where indicated, etoposide-treated cells were injected subcutaneously at the base of the foreleg into the opposite flank draining the axillary lymph node.

Cross-sectional area of tumors was measured in $mm^2$ using calipers every 2 to 3 days. In tumor re-challenge experiments, naïve mice controls or mice who had complete tumor regression and remained tumor free for at least 60 days were subcutaneously injected in the left flank (contra-lateral to the initial tumor) with $0.1 \times 10^6$ B16-Ova cells, and tumor development was monitored for another 60 days.

To enumerate circulating tumor antigen-specific $CD8^+$ T-cells, mice were bled retro-orbitally after the second intra-tumoral dose of PBS, etoposide, or etoposide-treated tumor cells, and H2-$K^b$/SIINFEKL-tetramer positive $CD8^+$ T cells analyzed by flow cytometry. Briefly, 50 μl of whole blood was collected by retro-orbital bleeding, centrifuged at 250 x g for 5 min, followed by 3 rounds of RBC lysis in 200 μl of ACK buffer. Cells were then washed once in Tetramer stain buffer (PBS containing 5 mM EDTA, 1% BSA and 50 nM dasatinib) and stained with PE-conjugated Tetramer for 40 min at room temperature followed by co-staining with antibody to CD8 for 10 min at 4°C. Cells were then stained with DAPI, washed, and re-suspended in tetramer stain buffer for flow cytometry analysis.

### Immunophenotyping

Phenotypic characterization of immune cell populations was performed by flow cytometry. Briefly, tumors were harvested and mashed through a 70 μM filter. Collected cells were washed in FACS buffer (PBS containing 5 mM EDTA and 1% BSA), resuspended, and counted. Five million cells from each sample were stained with fixable Live/Dead Aqua, stained with fluorophore-conjugated antibodies on ice for 30 min, washed, re-suspended in 450 μl, supplemented with 50 μl of CountBright absolute counting beads, and analyzed on a BD LSR Fortessa flow cytometer. DCs were scored as $CD45^{+}Ly6C^{-}CD24^{+}MHCII^{+}F480^{-}$ ($CD11b^{+}$ or $CD103^{+}$) cells using the gating strategy described in (30).

### Statistical analysis

All statistical analysis of data was performed using GraphPad Prism software. Comparisons of multiple experimental treatments to a single control condition were analyzed by ANOVA followed by Dunnett's multiple comparisons test. Comparisons between specific treatment groups were analyzed using a Student's *t*-test with Bonferroni correction for multiple hypothesis testing. For greater than three specific comparisons, ANOVA followed by Sidak's multiple comparisons test was used.

## Supplementary Material

Refer to Web version on PubMed Central for supplementary material.

## ACKNOWLEDGEMENTS:

We thank Lucia Suarez-Lopez, Jesse Patterson, Bert Van De Kooij, Dan Lim and Chris Barrett for many helpful discussions and the Koch Institute's Robert A. Swanson (1969) Biotechnology Center for technical support, including the Flow Cytometry and the Hope Babette Tang (1983) Histology core facilities.

**FUNDING:**

This study was supported in part by the NIH (R01-CA226898 and R35-ES028374 and to MBY), Cancer Center Support Grant P30-CA14051, Center for Environmental Health Support Grant P30-ES002109 as well as by awards to MBY from the Charles and Marjorie Holloway Foundation, the MIT Center for Precision Cancer Medicine and the Ovarian Cancer Research Foundation. This study was also supported by the Marble Center for Cancer Nanomedicine, the Koch Institute Frontier Research program (DJI), Mazumdar-Shaw International Oncology Fellowship to GS and the NIH Interdepartmental Biotechnology Training Program (T32-GM008334 to LEM). DJI is an investigator of the Howard Hughes Medical Institute.

## REFERENCES AND NOTES

1. American Cancer Society. Cancer Treatment & Survivorship Facts & Figures 2016-2017. Am Cancer Soc. 2016;
2. Ribas A, Wolchok JD. Cancer immunotherapy using checkpoint blockade. Science. 2018.
3. Larkin J, Chiarion-Sileni V, Gonzalez R, Grob JJ, Cowey CL, Lao CD, et al. Combined nivolumab and ipilimumab or monotherapy in untreated Melanoma. N Engl J Med. 2015;
4. Borghaei H, Paz-Ares L, Horn L, Spigel DR, Steins M, Ready NE, et al. Nivolumab versus docetaxel in advanced nonsquamous non-small-cell lung cancer. N Engl J Med. 2015;
5. Brahmer J, Reckamp KL, Baas P, Crinò L, Eberhardt WEE, Poddubskaya E, et al. Nivolumab versus docetaxel in advanced squamous-cell non-small-cell lung cancer. N Engl J Med. 2015;
6. Overman MJ, Bergamo F, McDermott RS, Aglietta M, Chen F, Gelsomino F, et al. Nivolumab in patients with DNA mismatch repair-deficient/microsatellite instability-high (dMMR/MSI-H)

metastatic colorectal cancer (mCRC): Long-term survival according to prior line of treatment from CheckMate-142. J Clin Oncol. 2018;

7. Overman MJ, McDermott R, Leach JL, Lonardi S, Lenz H-J, Morse MA, et al. Nivolumab in patients with metastatic DNA mismatch repair-deficient or microsatellite instability-high colorectal cancer (CheckMate 142): an open-label, multicentre, phase 2 study. Lancet Oncol Oncol. 2017;18(9).
8. Adams S, Schmid P, Rugo HS, Winer EP, Loirat D, Awada A, et al. Pembrolizumab monotherapy for previously treated metastatic triple-negative breast cancer: Cohort A of the phase II KEYNOTE-086 study. Ann Oncol. 2019;
9. Adams S, Loi S, Toppmeyer D, Cescon DW, De Laurentiis M, Nanda R, et al. Pembrolizumab monotherapy for previously untreated, PD-L1-positive, metastatic triple-negative breast cancer: Cohort B of the phase II KEYNOTE-086 study. Ann Oncol. 2019;
10. Nivolumab With or Without Ipilimumab in Treating Patients With Recurrent or High Grade Gynecologic Cancer With Metastatic Peritoneal Carcinomatosis [Internet]. Available from: https://clinicaltrials.gov/ct2/show/NCT03508570?term=nivolumab+ipilimumab+texas+ovarian&recrs=ae&cond=Ovarian+Cancer&rank=1
11. Pietzner K, Nasser S, Alavi S, Darb-Esfahani S, Passler M, Muallem MZ, et al. Checkpoint-inhibition in ovarian cancer: Rising star or just a dream? Journal of Gynecologic Oncology. 2018.
12. Eng C, Kim TW, Bendell J, Argilés G, Tebbutt NC, Di Bartolomeo M, et al. Atezolizumab with or without cobimetinib versus regorafenib in previously treated metastatic colorectal cancer (IMblaze370): a multicentre, open-label, phase 3, randomised, controlled trial. Lancet Oncol. 2019;
13. Haslam A, Prasad V. Estimation of the Percentage of US Patients With Cancer Who Are Eligible for and Respond to Checkpoint Inhibitor Immunotherapy Drugs. JAMA Netw open. 2019;
14. FDA approvalsHematology/Oncology (Cancer) Approvals & Safety Notifications. https://www.fda.gov/drugs/resources-information-approved-drugs/hematologyoncology-cancer-approvals-safety-notifications
15. Gandhi L, Rodríguez-Abreu D, Gadgeel S, Esteban E, Felip E, De Angelis F, et al. Pembrolizumab plus chemotherapy in metastatic non-small-cell lung cancer. N Engl J Med. 2018;
16. Burtness B, Harrington KJ, Greil R, Soulières D, Tahara M, de Castro G, et al. Pembrolizumab alone or with chemotherapy versus cetuximab with chemotherapy for recurrent or metastatic squamous cell carcinoma of the head and neck (KEYNOTE-048): a randomised, open-label, phase 3 study. Lancet. 2019;
17. Cortes J, Cescon DW, Rugo HS, Nowecki Z, Im SA, Yusof MM, et al. Pembrolizumab plus chemotherapy versus placebo plus chemotherapy for previously untreated locally recurrent inoperable or metastatic triple-negative breast cancer (KEYNOTE-355): a randomised, placebo-controlled, double-blind, phase 3 clinical trial. Lancet. 2020;
18. Cannell IG, Merrick KA, Morandell S, Zhu CQ, Braun CJ, Grant RA, et al. A Pleiotropic RNA-Binding Protein Controls Distinct Cell Cycle Checkpoints to Drive Resistance of p53-Defective Tumors to Chemotherapy. Cancer Cell. 2015;
19. Suarez-Lopez L, Sriram G, Kong YW, Morandell S, Merrick KA, Hernandez Y, et al. MK2 contributes to tumor progression by promoting M2 macrophage polarization and tumor angiogenesis. Proc Natl Acad Sci U S A. 2018;
20. Morandell S, Reinhardt HC, Cannell IG, Kim JS, Ruf DM, Mitra T, et al. A Reversible Gene-Targeting Strategy Identifies Synthetic Lethal Interactions between MK2 and p53 in the DNA Damage Response InVivo. Cell Rep. 2013;
21. Reinhardt HC, Hasskamp P, Schmedding I, Morandell S, van Vugt MATM, Wang XZ, et al. DNA damage activates a spatially distinct late cytoplasmic cell-cycle checkpoint network controlled by MK2-mediated RNA stabilization. Mol Cell. 2010;
22. Floyd SR, Pacold ME, Huang Q, Clarke SM, Lam FC, Cannell IG, et al. The bromodomain protein Brd4 insulates chromatin from DNA damage signalling. Nature. 2013;
23. Hsu AT, Barrett CD, DeBusk GM, Ellson CD, Gautam S, Talmor DS, et al. Kinetics and role of plasma matrix metalloproteinase-9 expression in acute lung injury and the acute respiratory distress syndrome. Shock. 2015;

24. Obeid M, Tesniere A, Ghiringhelli F, Fimia GM, Apetoh L, Perfettini JL, et al. Calreticulin exposure dictates the immunogenicity of cancer cell death. Nat Med. 2007;
25. Apetoh L, Ghiringhelli F, Tesniere A, Obeid M, Ortiz C, Criollo A, et al. Toll-like receptor 4-dependent contribution of the immune system to anticancer chemotherapy and radiotherapy. Nat Med. 2007;
26. T A, S F, B V, K O, M I, G F, et al. Immunogenic death of colon cancer cells treated with oxaliplatin. Oncogene. 2010.
27. Kepp O, Tartour E, Vitale I, Vacchelli E, Adjemian S, Agostinis P, et al. Consensus guidelines for the detection of immunogenic cell death. OncoImmunology. 2014.
28. Moynihan KD, Opel CF, Szeto GL, Tzeng A, Zhu EF, Engreitz JM, et al. Eradication of large established tumors in mice by combination immunotherapy that engages innate and adaptive immune responses. Nat Med. 2016;
29. Jutz S, Hennig A, Paster W, Asrak Ö, Dijanovic D, Kellner F, et al. A cellular platform for the evaluation of immune checkpoint molecules. Oncotarget. 2017;
30. Broz ML, Binnewies M, Boldajipour B, Nelson AE, Pollack JL, Erle DJ, et al. Dissecting the Tumor Myeloid Compartment Reveals Rare Activating Antigen-Presenting Cells Critical for T Cell Immunity. Cancer Cell. 2014;
31. Clarke SRmK, Barnden M, Kurts C, Carbone FR, Miller JF, Heath WR. Characterization of the ovalbumin-specific TCR transgenic line OT-I: MHC elements for positive and negative selection. Immunol Cell Biol. 2000;
32. Hogquist KA, Jameson SC, Heath WR, Howard JL, Bevan MJ, CF. T cell receptor antagonist peptides induce positive selection. Cell. 1994;76(1):17–27. [PubMed: 8287475]
33. Lin KY, Guarnieri FG, Staveley-O'Carroll KF, Levitsky HI, August JT, Pardoll DM, et al. Treatment of established tumors with a novel vaccine that enhances major histocompatibility class II presentation of tumor antigen. Cancer Res. 1996;
34. Bezu L, Gomes-da-Silva LC, Dewitte H, Breckpot K, Fucikova J, Spisek R, et al. Combinatorial strategies for the induction of immunogenic cell death. Frontiers in Immunology. 2015.
35. Silke J, Rickard JA, Gerlic M. The diverse role of RIP kinases in necroptosis and inflammation. Nat Immunol. 2015;
36. Li J, Yuan J. Caspases in apoptosis and beyond. Oncogene. 2008.
37. Liu T, Zhang L, Joo D, Sun SC. NF-κB signaling in inflammation. Signal Transduction and Targeted Therapy. 2017.
38. Obata T, Brown GE, Yaffe MB. Map kinase pathways activated by stress: The p38 MAPK pathway. Critical Care Medicine. 2000.
39. Pierce JW, Schoenleber R, Jesmok G, Best J, Moore SA, Collins T, et al. Novel inhibitors of cytokine-induced IκBα phosphorylation and endothelial cell adhesion molecule expression show anti-inflammatory effects in vivo. J Biol Chem. 1997;
40. Davies SP, Reddy H, Caivano M, Cohen P. Specificity and mechanism of action of some commonly used protein kinase inhibitors. Biochem J. 2000;
41. Reyhanoglu G, Tadi P. Etoposide. StatPearls [Internet] Treasure Isl StatPearls Publ [Internet]. 2021; Available from: https://www.ncbi.nlm.nih.gov/books/NBK557864/
42. Edelson BT, Wumesh KC, Juang R, Kohyama M, Benoit LA, Klekotka PA, et al. Peripheral CD103+ dendritic cells form a unified subset developmentally related to CD8α+ conventional dendritic cells. J Exp Med. 2010;
43. Merad M, Sathe P, Helft J, Miller J, Mortha A. The Dendritic Cell Lineage: Ontogeny and Function of Dendritic Cells and Their Subsets in the Steady State and the Inflamed Setting. Annu Rev Immunol. 2013;
44. Hildner K, Edelson BT, Purtha WE, Diamond M, Matsushita H, Kohyama M, et al. Batf3 deficiency reveals a critical role for CD8α + dendritic cells in cytotoxic T cell immunity. Science (80- ). 2008;
45. Casares N, Pequignot MO, Tesniere A, Ghiringhelli F, Roux S, Chaput N, et al. Caspase-dependent immunogenicity of doxorubicin-induced tumor cell death. J Exp Med. 2005;

46. Matsuoka S, Ballif BA, Smogorzewska A, McDonald ER, Hurov KE, Luo J, et al. ATM and ATR substrate analysis reveals extensive protein networks responsive to DNA damage. Science (80- ). 2007;
47. Pfirschke C, Engblom C, Rickelt S, Cortez-Retamozo V, Garris C, Pucci F, et al. Immunogenic Chemotherapy Sensitizes Tumors to Checkpoint Blockade Therapy. Immunity. 2016;
48. Ghiringhelli F, Apetoh L, Tesniere A, Aymeric L, Ma Y, Ortiz C, et al. Activation of the NLRP3 inflammasome in dendritic cells induces IL-1B-dependent adaptive immunity against tumors. Nat Med. 2009;
49. Yatim N, Jusforgues-Saklani H, Orozco S, Schulz O, Da Silva RB, Reis E Sousa C, et al. RIPK1 and NF-kB signaling in dying cells determines cross-priming of CD8+ T cells. Science (80- ). 2015;
50. Snyder AG, Hubbard NW, Messmer MN, Kofman SB, Hagan CE, Orozco SL, et al. Intratumoral activation of the necroptotic pathway components RIPK1 and RIPK3 potentiates antitumor immunity. Sci Immunol. 2019;
51. Bock FJ, Tait SWG. Mitochondria as multifaceted regulators of cell death. Nature Reviews Molecular Cell Biology. 2020.
52. Giampazolias E, Zunino B, Dhayade S, Bock F, Cloix C, Cao K, et al. Mitochondrial permeabilization engages NF-κB-dependent anti-tumour activity under caspase deficiency. Nat Cell Biol. 2017;
53. Steinman RM, Witmer MD. Lymphoid dendritic cells are potent stimulators of the primary mixed leukocyte reaction in mice. Proc Natl Acad Sci U S A. 1978;
54. Peterson JR, Ora A, Nguyen Van P, Helenius A. Transient, lectin-like association of calreticulin with folding intermediates of cellular and viral glycoproteins. Mol Biol Cell. 1995;
55. Wada I, Kai M, Imai S, Sakane F, Kanoh H. Promotion of transferrin folding by cyclic interactions with calnexin and calreticulin. EMBO J. 1997;
56. Nauseef WM, McCormick SJ, Clark RA. Calreticulin functions as a molecular chaperone in the biosynthesis of myeloperoxidase. J Biol Chem. 1995;
57. Yang Y, Xia F, Hermance N, Mabb A, Simonson S, Morrissey S, et al. A Cytosolic ATM/NEMO/RIP1 Complex Recruits TAK1 To Mediate the NF- B and p38 Mitogen-Activated Protein Kinase (MAPK)/MAPK-Activated Protein 2 Responses to DNA Damage. Mol Cell Biol. 2011;
58. Wu G, Song L, Zhu J, Hu Y, Cao L, Tan Z, et al. An ATM/TRIM37/NEMO axis counteracts genotoxicity by activating nuclear-to-cytoplasmic NF-kB signaling. Cancer Res. 2018;
59. Biton S, Ashkenazi A. NEMO and RIP1 control cell fate in response to extensive DNA damage via TNF-α feedforward signaling. Cell. 2011;
60. Tentner AR, Lee MJ, Ostheimer GJ, Samson LD, Lauffenburger DA, Yaffe MB. Combined experimental and computational analysis of DNA damage signaling reveals context-dependent roles for Erk in apoptosis and G1/S arrest after genotoxic stress. Mol Syst Biol. 2012;
61. Gasser S, Orsulic S, Brown EJ, Raulet DH. The DNA damage pathway regulates innate immune system ligands of the NKG2D receptor. Nature. 2005;
62. Holler N, Zaru R, Micheau O, Thome M, Attinger A, Valitutti S, et al. Fas triggers an alternative, caspase-8-independent cell death pathway using the kinase RIP as effector molecule. Nat Immunol. 2000;
63. Degterev A, Huang Z, Boyce M, Li Y, Jagtap P, Mizushima N, et al. Chemical inhibitor of nonapoptotic cell death with therapeutic potential for ischemic brain injury. Nat Chem Biol. 2005;
64. Spranger S, Dai D, Horton B, Gajewski TF. Tumor-Residing Batf3 Dendritic Cells Are Required for Effector T Cell Trafficking and Adoptive T Cell Therapy. Cancer Cell. 2017;
65. Roberts EW, Broz ML, Binnewies M, Headley MB, Nelson AE, Wolf DM, et al. Critical Role for CD103+/CD141+ Dendritic Cells Bearing CCR7 for Tumor Antigen Trafficking and Priming of T Cell Immunity in Melanoma. Cancer Cell. 2016;
66. Barry KC, Hsu J, Broz ML, Cueto FJ, Binnewies M, Combes AJ, et al. A natural killer–dendritic cell axis defines checkpoint therapy–responsive tumor microenvironments. Nat Med. 2018;
67. Matzinger P The danger model: A renewed sense of self. Science. 2002.

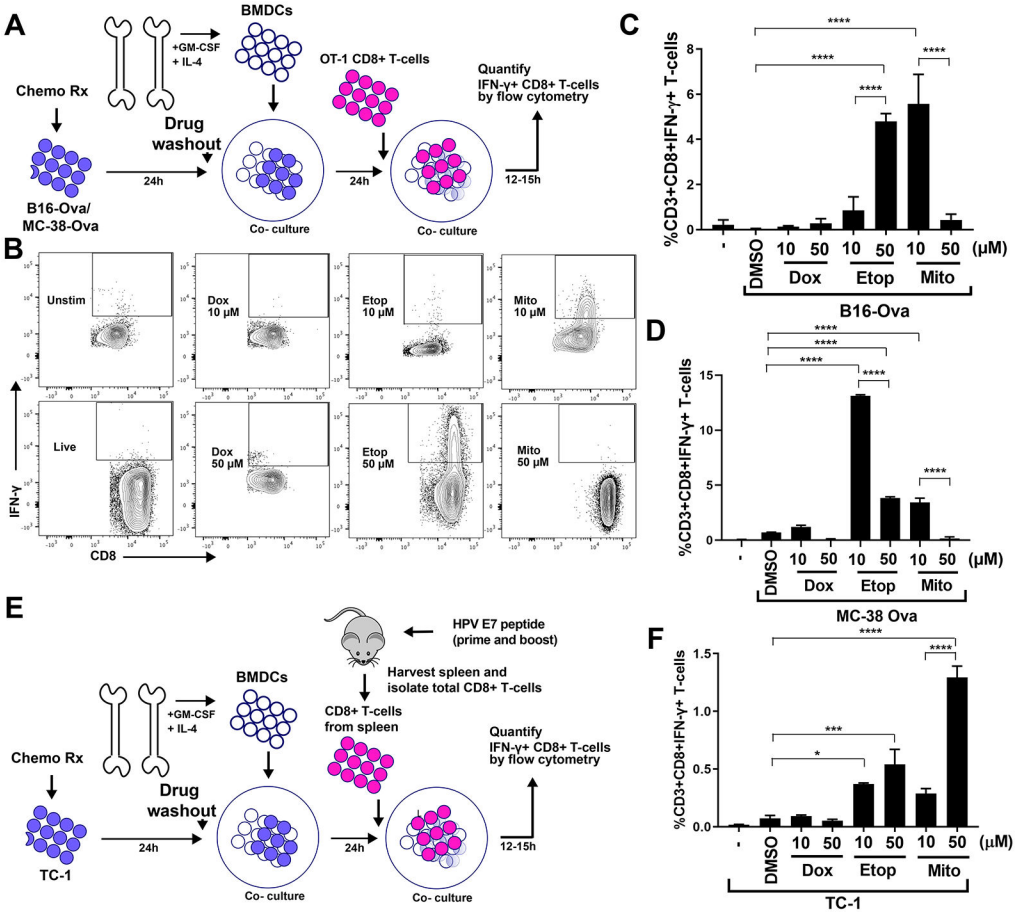


**Figure 1: An experimental system to assess DC-mediated T cell IFN-γ responses to genotoxically damaged tumor cells.**

**(A)** Schematic of the in vitro experimental system. B16-Ova or MC-38-Ova cells were treated with DNA-damaging agents for 24 hours, washed and incubated with primary bone marrow-derived dendritic cells (BMDC) for another 24 hours. Following this, OT-I $CD8^+$ T cells expressing a TCR transgene that specifically recognizes the Ova-derived peptide SIINFEKL in the context of $H2\text{-}K^b$ (OT-1) (31,32) were added and evaluated for intracellular IFN-γ 15 hours later. **(B)** T cells resulting from the experimental protocol described in (A) were identified by CD3 staining, and re-gated for IFN-γ and CD8 expression. Representative flow cytometry plots assessing IFN-$\gamma^+$ $CD8^+$ T cell populations (boxed region) induction by treatment of B16-Ova cells with 10 μM or 50 μM of doxorubicin, etoposide, or mitoxantrone. **(C and D)** Quantification of BMDC-mediated induction of IFN-$\gamma^+$ $CD8^+$ T-cells from 5 (C) or 3 (D) independent experiments with B16-Ova and MC-38-Ova cells, respectively, described in (A and B). The first lane marked "-" indicates the percen67age of IFN-$\gamma^+$ $CD8^+$ T cells produced by co-culture of BMDCs and T cells in the absence of tumor cells. **(E)** Schematic of the in vitro experimental system using TC-1 cells, treated co-cultured with BMDCs as described in (A), then co-cultured with $CD8^+$ T cells isolated from mice vaccinated (primed and boosted) with an HPV-E7 peptide. As in (A), T cells were then assessed for intracellular IFN-γ 15 hours later. **(F)** Quantification of IFN-$\gamma^+$ $CD8^+$ T cells from 3 experiments described in (E). "-" as

described for (C and D). For all the above panels, error bars indicate SEM, *$P$<0.05, ***$P$<0.005, and ****$P$<0.0001 by ANOVA followed by Sidak's multiple comparisons test.

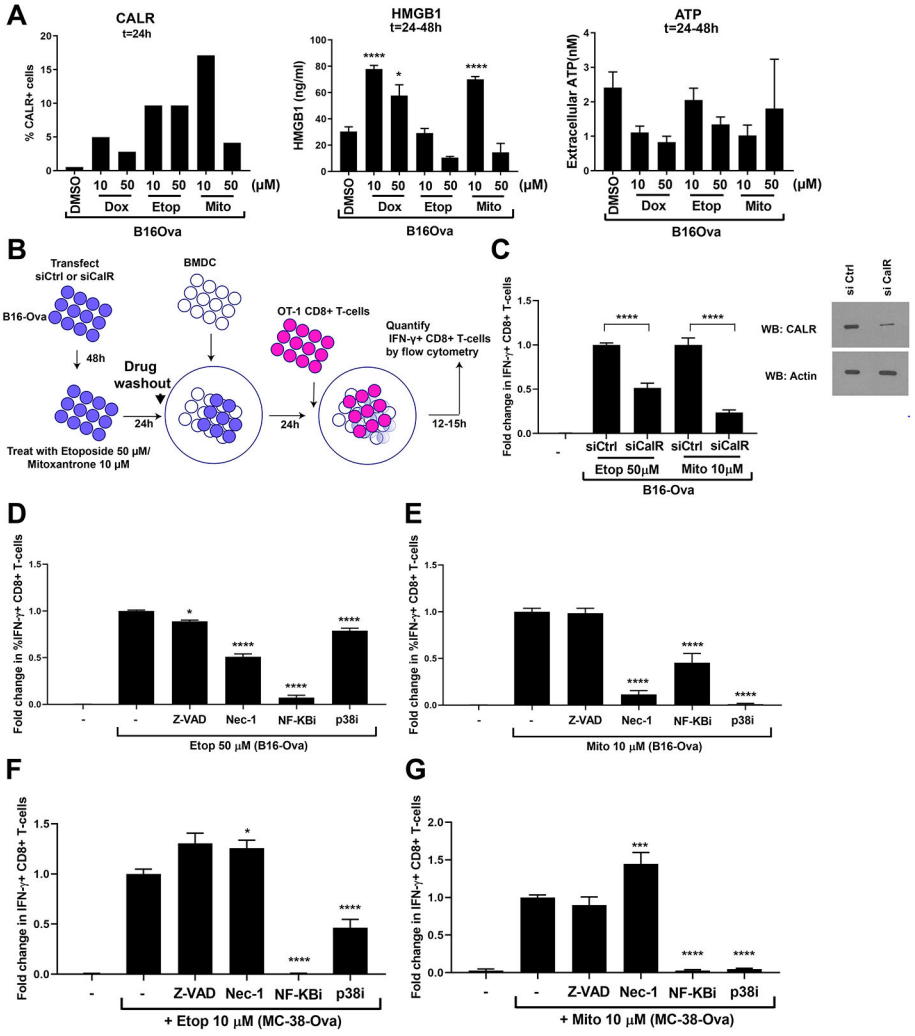


**Figure 2: T-cell IFN-γ responses by DNA-damaged tumor cells involves calreticulin and signaling through NF-κB, p38 MAPK and RIPK1.**

**(A)** Left, percentage of B16-Ova tumor cells displaying surface calreticulin 24 hours after the indicated treatment from a representative of two experiments. Results from an additional representative experiment using a second antibody is shown in fig. S2A. Middle and right, levels of HMGB1 and ATP in the culture media measured 24 to 48 hours after the indicated treatment. Results are from 4 independent experiments, with error bars indicating SEM. **P*<0.05, ***P*<0.01, ****P*<0.005, and *****P*<0.0001 compared to DMSO-treated control by ANOVA followed by Dunnett's multiple comparisons test. "ns" indicates *P*>0.05 by one-way ANOVA. **(B)** Schematic of the siRNA experiment testing the role of B16-Ova cell calreticulin in BMDC-mediated IFN-γ induction in T cells. **(C)** Left, quantification of the fold change in %IFN-$\gamma^+$ $CD8^+$ T-cells from the experiment in (B). Data for each calreticulin knockdown condition is normalized to the respective drug-treated control knockdown condition. Results represent 3 independent experiments with error bars indicating SEM. Data were analyzed by ANOVA followed by Sidak's multiple comparisons test comparing drug-treated knockdown to drug-treated controls. * *P*<0.05 and **** *P*<0.0001. Right, quantification of calreticulin knockdown efficiency by Western blotting. First lane, "-",

defined as in Fig. 1C. **(D to G)** Quantification of the fold change in %IFN-$\gamma^+$ $CD8^+$ T cells induced by BMDC after incubation with etoposide- or mitoxantrone-treated B16-Ova (D and E) or MC-38-Ova (F and G) cells that were co-treated with the indicated DNA damaging agent plus either Z-VAD, necrostatin-1 (Nec-1), Bay 11-7085 (inhibitor of NF-κB signaling) or SB202190 (p38 MAPK inhibitor). First lane (−) defined as in Fig. 1C. Data are normalized to the condition in which B16-Ova cells are treated with etoposide alone or mitoxantrone alone, respectively. Results from 3 independent experiments with error bars indicating SEM. *$P$<0.05 and ****$P$<0.0001 wherein each co-treatment condition (etoposide or mitoxantrone + either Z-VAD, Nec-1, NF-κBi or p38i) is compared with the etoposide or mitoxantrone alone condition using ANOVA followed by Dunnett's multiple comparisons test.

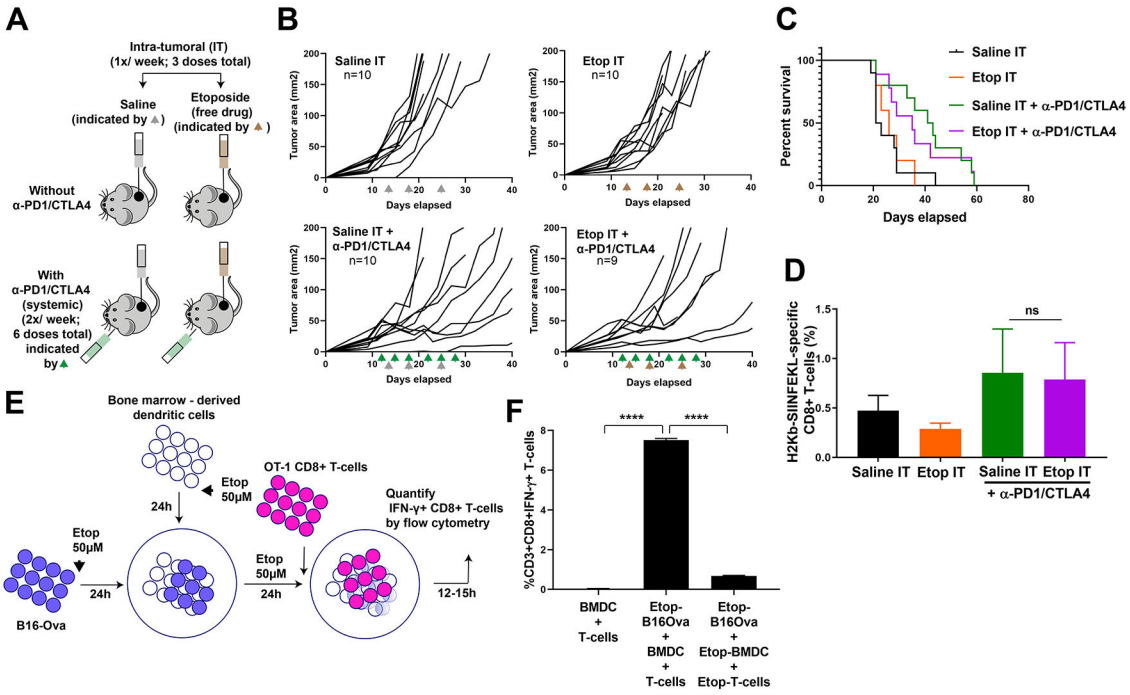


**Fig. 3: Direct intra-tumoral administration of etoposide does not synergize with ICB.**

**(A)** Schematic of the experimental design and dosing regimen used for testing intra-tumoral administration of etoposide in the presence or absence of systemic anti-PD1 and anti-CTLA4. **(B)** Tumor growth curves in mice bearing B16-Ova tumors treated with intra-tumoral saline (Saline IT; gray arrowheads) or etoposide (Etop IT; brown arrowheads) in the presence or absence of systemic anti-PD1 and anti-CTLA4 (green arrowheads). The number of mice in each group is indicated. One mouse in the Etop IT + anti-PD1/CTLA4 group did not show tumor growth beyond 4mm$^2$ throughout the experiment and was excluded. **(C)** Kaplan-Meier survival curves of the experiment in (B), compared by log-rank test. **(D)** Frequency of circulating H2-K$^b$/SIINFEKL -specific CD8$^+$ T cells from mice treated with the conditions indicated. Error bars represent SEM. The frequency of H2-K$^b$/SIINFEKL tetramer stained CD8$^+$ T cells in the Etop IT + anti-PD1/CTLA4 treatment group was not significantly different from that of the Saline IT + anti-PD1/CTLA4 group (one-tailed *t*-test, $P$=0.4553 indicated by “ns”). **(E)** Schematic of the experiment examining etoposide co-treatment of BMDC, T cells, and B16-Ova cells. **(F)** Quantification of IFN-γ$^+$ CD8$^+$ T cells (from 3 independent experiments) induced by BMDC after co-culture with etoposide-treated B16-Ova cells when both BMDC and T-cells were exposed to etoposide compared to when only B16-Ova cells were exposed. Error bars represent SEM. ****$P$<0.0001 by ANOVA followed by Sidak’s multiple comparisons test.

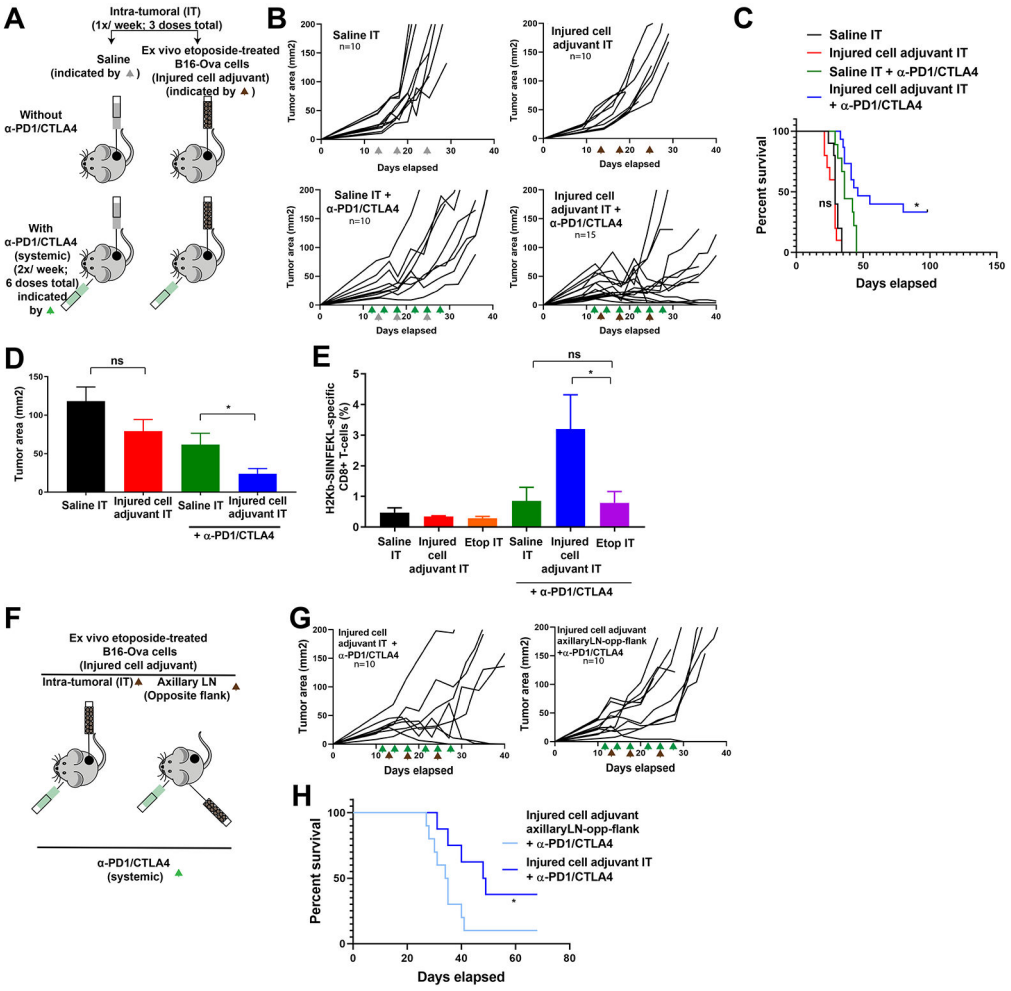


**Figure 4: Intra-tumoral administration of ex vivo DNA-damaged tumor cells plus systemic ICB expands CD8$^+$ T-cells and increases tumor control and survival.**

**(A)** Schematic of the experimental design and dosing regimen used for testing intra-tumoral administration of etoposide-treated B16-Ova cells (injured cell adjuvant) in the presence or absence of systemic anti-PD1 and anti-CTLA4. **(B)** Tumor growth curves for mice treated with intra-tumoral saline (Saline IT; gray arrowheads) or ex vivo etoposide-treated B16-Ova cells (Injured cell adjuvant IT; brown arrowheads) in the presence or absence of systemic anti-PD1 and anti-CTLA4 (green arrowheads). “n” indicates the number of mice in each group. **(C)** Kaplan-Meier Survival curves of the experiment in (B). *$P$<0.05 by log-rank test compared to the Saline IT + anti-PD1/CTLA4 group. “ns”, $P$>0.05. **(D)** Average tumor cross-sectional area on day 21 for each treatment group. Error bars indicate SEM. *$P$<0.05 and “ns” $P$>0.05 by one-tailed $t$-tests. **(E)** Frequency of circulating H2-K$^b$/SIINFEKL -specific CD8$^+$ T cells from mice after the indicated treatments. *$P$<0.05 and “ns” $P$>0.05 by ANOVA followed by Sidak’s multiple comparisons test. **(F)** Schematic of the experimental design and dosing regimen used for testing intra-tumoral administration versus contralateral flank administration (draining the axillary lymph node) of etoposide-treated B16-Ova cells (injured cell adjuvant) in combination with systemic anti-PD1 and anti-CTLA4. This was done independently of the cohorts used in (B, C, D and E). **(G)** Tumor growth curves for

mice treated with intra-tumoral (IT) or distant lymph node (axillary LN, opposite flank) injection of ex vivo etoposide-treated B16-Ova cells (Injured cell adjuvant) in combination with systemic anti-PD1 and anti-CTLA4. “n” indicates the number of mice in each group. **(H)** Kaplan-Meier Survival curves of the experiment in (G). *$P$<0.05 by log-rank test.

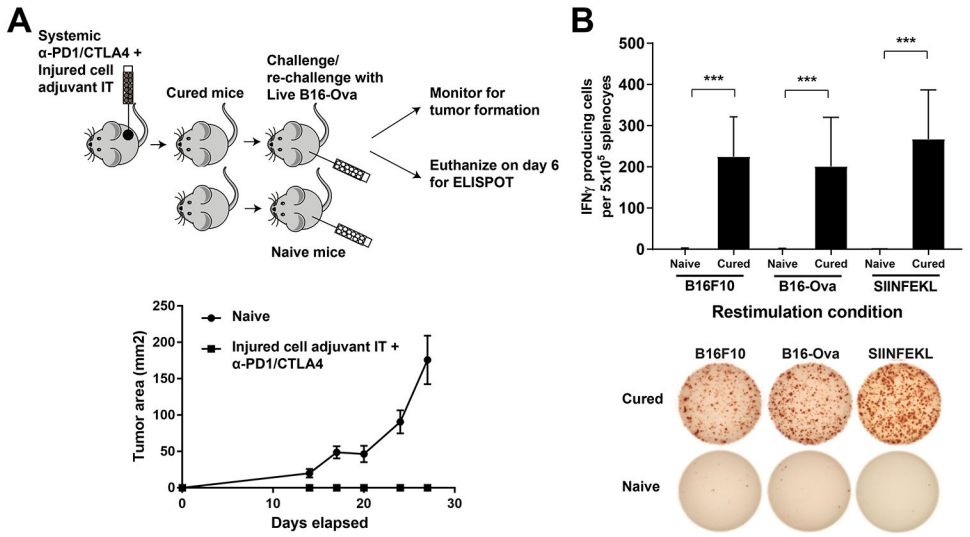


**Figure 5: Long-term immunological memory and CD8$^+$ T cell responses towards non-Ova antigens are induced by the injured cell adjuvant plus ICB.**

**(A)** Top, schematic of the re-challenge experiment to monitor tumor growth, and a separate re-challenge experiment in an independent cohort for ELISPOT. To monitor tumor growth, 5 naïve mice and 5 mice that demonstrated complete tumor regression following treatment with injured cell adjuvant + systemic anti-PD1/CTLA4 were re-challenged in the opposite flank with 100,000 live B16-Ova cells. For ELISPOT, an independent cohort of mice that demonstrated complete tumor regression following treatment with injured cell adjuvant + systemic anti-PD1/CTLA4 were re-challenged with 100,000 live B16-Ova cells. On Day 6 after re-challenge, spleens were harvested and splenocytes were re-stimulated with either B16-F10, B16-Ova cells or with purified SIINFEKL peptide. Spleens from naïve mice were also re-stimulated as above. Bottom, resulting tumor growth curves from the re-challenge experiment (on 5 cured mice derived from three independent experiments) to monitor tumor growth. Error bars indicate SEM. **(B)** Top, quantification of ELISPOT results (from 5 cured mice derived from three independent experiments) expressed as IFN-γ–producing cells per $10^5$ splenocytes. Error bars indicate SEM. ***$P$<0.005 by two-way ANOVA. Bottom, representative images from the ELISPOT plate for the conditions in the top panel.

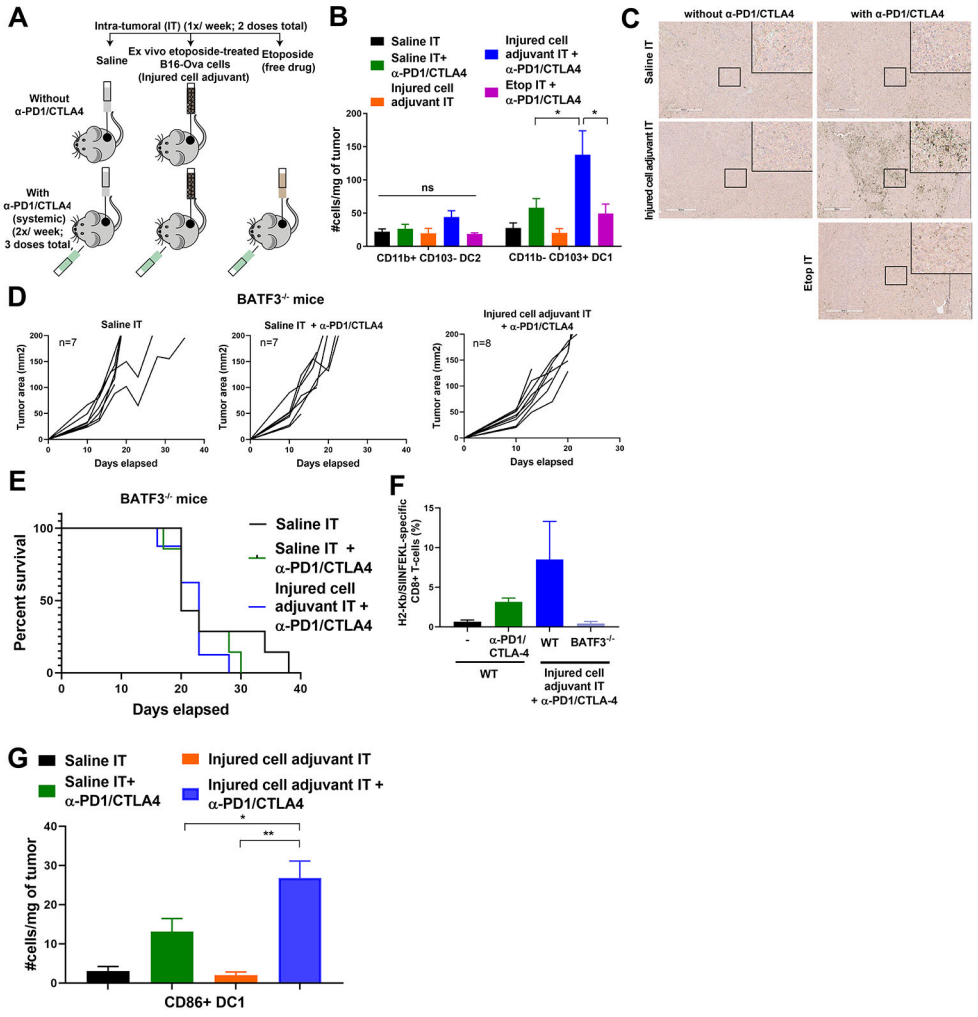


**Figure 6: Intra-tumoral administration of the injured cell adjuvant plus systemic ICB increases DC1 density in the tumor and requires BATF3 for efficacy.**

**(A)** Schematic of the experimental design and dosing regimen used to test the effect of intra-tumoral etoposide-treated B16-Ova cells in combination with systemic anti-PD1/CTLA4 on the frequency of intra-tumoral DC. **(B)** Quantification of intra-tumoral CD11b-CD103+ DC1 and CD11b$^{+}$CD103$^{-}$ DC2 subsets from treated tumors analyzed by flow cytometry (5 mice per group). Error bars represent SEM. * $P$<0.05 by ANOVA followed by Sidak's multiple comparisons test. "ns" indicates $P$>0.05 by ANOVA. **(C)** Tumor sections were stained with an antibody to BATF3. Insets show higher-magnification images of the boxed central region of each section. Scale bar, 400 μm. **(D)** Tumor growth curves of *Batf3*$^{-/-}$ mice treated with intra-tumoral saline or etoposide-treated B16-Ova cells (injured cell adjuvant) in combination with systemic anti-PD1 and anti-CTLA4 antibodies. "n" indicates the number of mice in each group. **(E)** Kaplan-Meier survival curves of the experiment in (D). $P$=0.5220 by log-rank test. **(F)** Frequency of circulating H2-K$^{b}$/SIINFEKL specific CD8$^{+}$ T cells from WT and *Batf3*$^{-/-}$ mice treated as indicated. **(G)** Quantification of intra-tumoral CD86$^{+}$ DC1 from tumors treated 24 hours prior with one dose of saline or injured cell adjuvant (IT) in presence or absence of one dose of systemic anti-PD1 and anti-CTLA4 48 hours prior.

Error bars represent SEM, 5 mice per group. *$P$<0.05 and **$P$<0.01 by ANOVA followed by Sidak's multiple comparisons test.

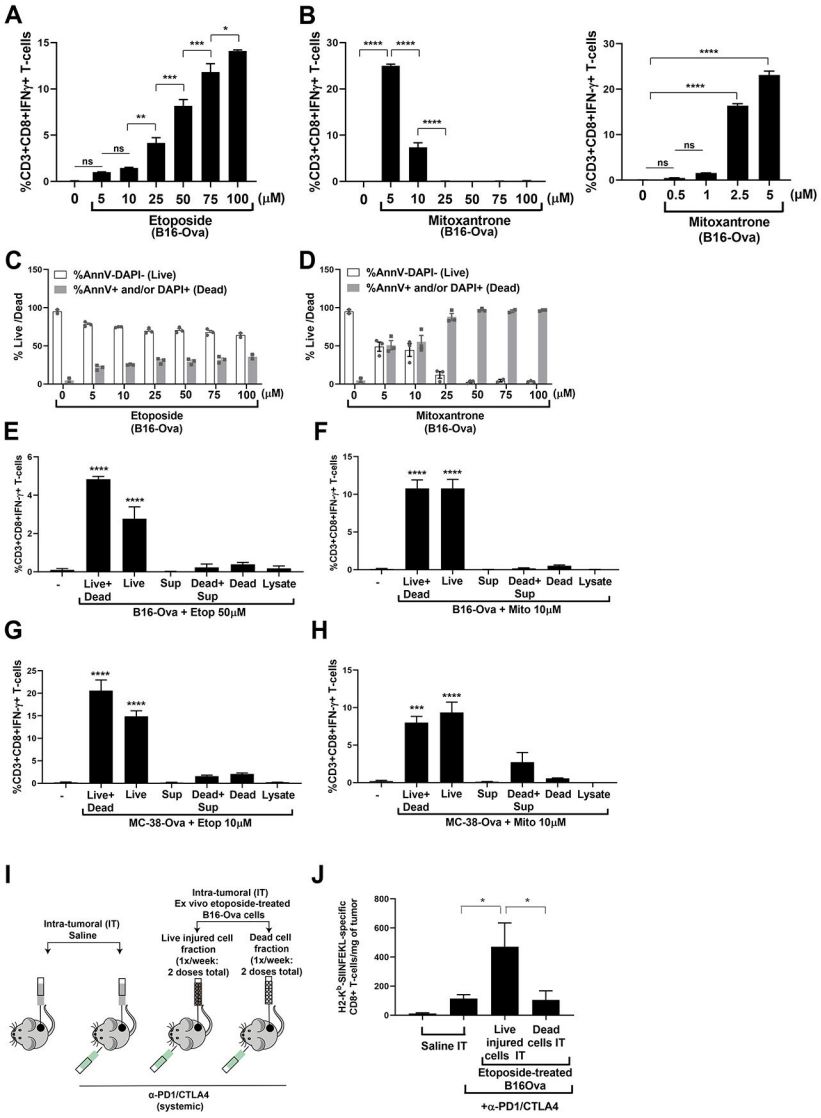


**Figure 7: Live injured cells, rather than dead cells, are the primary determinants of DC-mediated T cell IFN-γ responses.**

**(A and B)** Quantification from three independent experiments of IFN-γ+ $CD8^+$ T-cells induced by co-culture of BMDC with B16-Ova cells treated with etoposide (A) or mitoxantrone (B) at the indicated concentrations for 24 hours. The first lane (−) indicates the percentage of IFN-$\gamma^+$ $CD8^+$ T cells produced by co-culture of BMDCs and T-cells in the absence of B16-Ova cells. Error bars indicate SEM. **P*<0.05, ***P*<0.01, ****P*<0.005, *****P*<0.0001, and "ns" *P*>0.05 by ANOVA followed by Sidak's (A and B, left) or Dunnett's (B, right) multiple comparisons test. **(C and D)** Quantification from two to three independent experiments of the proportion of live (AnnV and DAPI double negative; white bars) and dead (sum total of AnnV and/or DAPI single or double positive; grey bars) cells after treatment of B16-Ova cells for 24 hours with etoposide or mitoxantrone as indicated. Data points are shown with means ± SEM; where N=2, error bars indicate range. **(E and F)** Quantification from three independent experiments of IFN-$\gamma^+$ $CD8^+$ T cells induced by co-culture of BMDC with the indicated B16-Ova **(E and F)** or MC-38-**Ova (G and H)**

live cell ($AnnV^{-}/DAPI^{-}$) and dead cell fractions obtained after treatment with etoposide (50 μM) or mitoxantrone (10 μM). "-", controls. BMDC was co-cultured with each of the fractions or combinations thereof for 24 hours before OT-1 $CD8^{+}$ T cells were added. Live+dead, whole treated cell mixture; Live, live cell fraction; Dead, dead cell fraction; Sup, cell-free supernatant; Dead+Sup, dead cells combined with cell-free supernatant. Error bars indicate SEM. ***$P$<0.005, and ****$P$<0.0001 by ANOVA followed by Dunnett's multiple comparisons test. **(I)** Schematic of the experimental design and dosing regimen used to test the effect of intra-tumoral administration of etoposide-treated B16-Ova cells in combination with systemic anti-PD1/CTLA4 on the frequency of intra-tumoral H2-$K^{b}$/SIINFEKL–specific $CD8^{+}$ T-cells. Dosing frequency of saline, live or dead fractions of ex vivo etoposide-treated B16-Ova cells (IT) and systemic anti-PD1 and anti-CTLA4 was as shown in Fig. 6A. Tumors were harvested 2 days after the second dose of injured cell adjuvant. **(J)** Frequency of intra-tumoral H2-$K^{b}$/SIINFEKL–specific $CD8^{+}$ T cells from tumors treated with the conditions indicated (four to five mice per group). Error bars represent SEM. *$P$<0.05 by ANOVA followed by Sidak's multiple comparisons test.

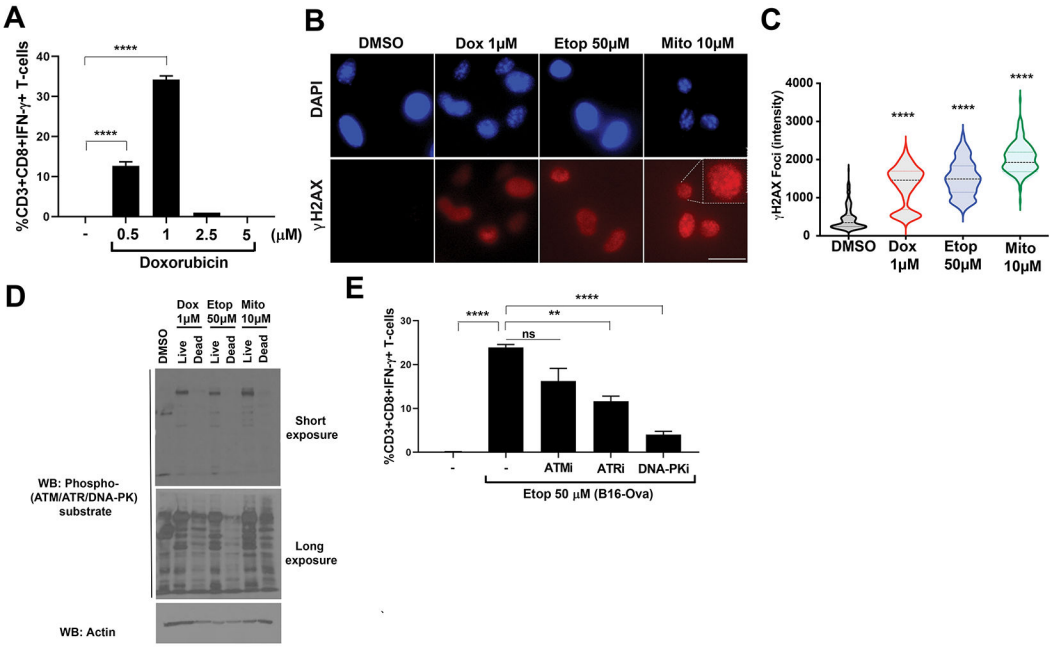


**Figure 8: Live injured chemotherapy-treated tumor cells require DNA-damage signaling for the DC-mediated T cell IFN-γ response.**

**(A)** B16-Ova cells were treated with doxorubicin at 0.5, 1, 2.5 or 5 μM for 24 hours, washed, and incubated with primary bone marrow-derived dendritic cells (BMDC) for another 24 hours. Following this, OT-I $CD8^+$ T cells were added and evaluated for intracellular IFN-$\gamma$ 15 hours later. Quantification of IFN-$\gamma^+$ $CD8^+$ T-cells from three independent experiments is shown. Error bars represent SEM. ****$P$<0.0001 by ANOVA followed by Dunnett's multiple comparisons test. **(B)** B16-Ova cells were treated with doxorubicin, etoposide, or mitoxantrone at the doses indicated for 24 hours and the live (attached) fractions were analyzed by fluorescence microscopy after staining with DAPI (blue channel) and anti-γH2AX (red channel). Representative images are shown. Scale bar, 20 μm. **(C)** Quantification of γH2AX foci intensity from the experiment in (B) is shown. n ≥ 200 cells per condition. Width in violin plot indicates frequency for each observed value from maximum to minimum, with dotted line indicating median. ****$P$<0.0001 by ANOVA followed by Dunnett's multiple comparisons test compared to the DMSO control. **(D)** B16-Ova cells were treated with doxorubicin, etoposide, or mitoxantrone at the doses indicated for 24 hours followed by separation of the live and dead fractions and analysis of respective lysates by Western blotting. Blots are representative of two independent experiments. **(E)** Quantification of IFN-$\gamma^+$ $CD8^+$ T cells (from three independent experiments) induced by BMDC following incubation with B16-Ova cells that were co-treated with 50 μM etoposide and 10 μM of either ATM kinase inhibitor KU-55933, ATR kinase inhibitor AZD6738 or DNA-PK inhibitor NU7441. First lane (−) defined as in Fig. 1C. Error bars represent SEM. **$P$<0.01 and ****$P$<0.0001 by ANOVA followed by Dunnett's multiple comparisons test versus the "Etop 50 μM" group.

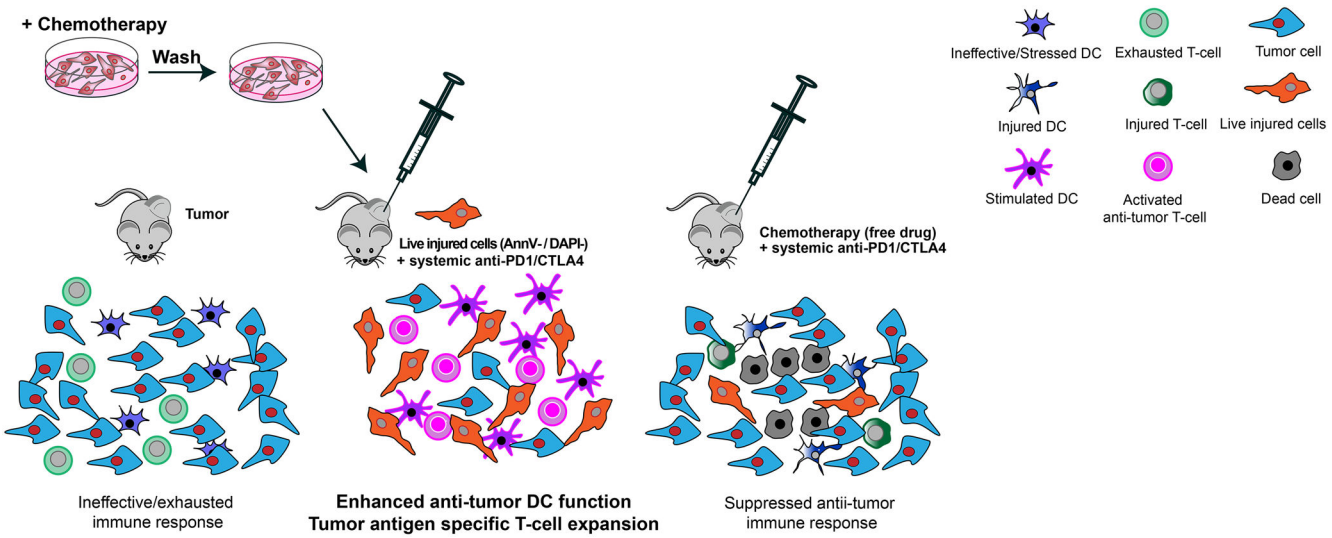


**Figure 9: Model of immunogenic cell injury generating anti-tumor immunity.**

Intra-tumoral injection of tumor cells treated ex vivo with DNA-damaging chemotherapy promotes effective DC-mediated T cell priming and expansion when combined with systemic immune checkpoint blockade. Neither cell-free supernatants, the dead cell fraction, nor lysates of the chemotherapy-treated tumor cells generated by three cycles of freeze-thawing, when co-incubated with DC, promoted a T cell IFN-γ response, indicating that some type of active cellular process beyond cytokine secretion from genotoxically injured tumor cells is likely involved. Furthermore, if the DCs and/or T cells were also exposed to the cytotoxic chemotherapy drug, T cell IFN-γ responses were impaired. Consequently, direct intra-tumoral injection of the free chemotherapeutic drug, in combination with systemic ICB administration, was largely ineffective at inducing an anti-tumor immunogenic response.